

RESEARCH

Open Access



SIRP α modulates microglial efferocytosis and neuroinflammation following experimental subarachnoid hemorrhage via the SHP1/STAT6 axis

Bingtao Zhang^{1†}, Yan Zou^{1†}, Qikai Tang^{1†}, Zixuan Yuan^{2†}, Kun Jiang³, Zhaoxiang Zhang³, Shujuan Chen¹, Qi Wu¹, Xiaoming Zhou^{1*} and Xin Zhang^{1*}

Abstract

Subarachnoid hemorrhage induces extensive neuronal cell death, leading to the release of damage-associated molecular patterns (DAMPs). These DAMPs, along with hemoglobin and cell corpses, trigger localized inflammation. Signal regulatory protein alpha (SIRP α) plays a crucial role in efferocytosis by acting as a “don’t eat-me” signal, modulating inflammation and tissue homeostasis. However, the precise function and regulatory mechanisms of SIRP α in efferocytosis remain unclear. Proteomic analysis of cerebrospinal fluid (CSF) reveals that SIRP α levels are significantly elevated in the CSF of SAH patients and correlate with clinical outcomes. In vivo and in vitro studies show that microglial knockdown of SIRP α promotes efferocytosis and attenuates neuroinflammation following SAH. SIRP α inhibits efferocytosis by recruiting and phosphorylating SHP1 and SHP2 through phosphorylation of four tyrosine residues in its cytoplasmic domain, with SHP1 playing a particularly critical role. Mutation of these tyrosine residues to non-phosphorylatable alanine residues enhances efferocytosis and reduces neuroinflammation in vitro. RNA-seq analysis suggests that this mutation upregulates the expression of “eat-me” signals, MerTK and CD36, and identifies STAT6 as a key transcription factor involved in this process. In conclusion, SIRP α plays a central role in regulating microglia efferocytosis and neuroinflammation after SAH via the SHP1/STAT6 axis. Targeting this pathway may provide a promising therapeutic approach for SAH.

Keywords Subarachnoid hemorrhage, Neuroinflammation, Efferocytosis, Signal regulatory protein alpha, Signal transducer and activator of transcription 6

[†]Bingtao Zhang, Yan Zou, Qikai Tang and Zixuan Yuan contributed equally to this work.

*Correspondence:
Xiaoming Zhou
xiaoming20111386@163.com
Xin Zhang
zhangxsp@163.com

¹Department of Neurosurgery, Nanjing Jinling Hospital, Affiliated Hospital of Medical School, Nanjing University, Nanjing, China

²Department of Neurosurgery, Jiangsu Province Hospital of Chinese Medicine, Affiliated Hospital of Nanjing University of Chinese Medicine, Nanjing, China

³Department of Neurosurgery, Jinling Hospital, Nanjing Medical University, Nanjing, China



Introduction

Subarachnoid hemorrhage (SAH) is a specific type of stroke primarily resulting from the rupture of intracranial aneurysms, which account for approximately 5% of all strokes. This condition is associated with high mortality and morbidity rates [1]. Despite significant advancements in pharmacological, microsurgical, and endovascular interventions, the mortality and morbidity rates among SAH patients remain elevated, posing substantial challenges to individuals and society [2, 3]. The pathophysiological mechanisms underlying SAH can be categorized into early brain injury (EBI), occurring within 72 h of onset, and delayed cerebral ischemia (DCI), which manifests between 3 and 15 days post-onset [4]. Early research indicated that DCI is a primary contributor to poor outcomes in SAH patients; however, therapeutic approaches targeting DCI have not yielded substantial improvements in patient recovery. Consequently, recent investigations have increasingly concentrated on EBI [5, 6]. The pathophysiological mechanisms of EBI following SAH encompass neuroinflammation, neuronal oxidative stress, apoptosis, blood-brain barrier (BBB) disruption, and microthrombosis resulting from direct blood exposure and global ischemia-hypoxia [7, 8].

Efferocytosis, the phagocytic removal and recycling of dead/dying cells by specialized phagocytes at specific sites, is pivotal in regulating inflammatory responses and facilitating tissue repair [9]. The stimulation of toxic substances and global ischemia-hypoxia lead to neuronal cell death via mechanisms such as apoptosis, pyroptosis, and ferroptosis, with apoptosis being the most prominent [10, 11]. Following blood enters into subarachnoid space, extensive cell death results in the release of damage-associated molecular patterns (DAMPs). These DAMPs, along with hemoglobin and cellular corpses, trigger localized inflammation [12, 13]. Simultaneously, apoptotic cells (ACs) release “find-me” signals that recruit phagocytes especially microglia to the injury site, binding with the “eat-me” signals on the membrane to promote the engulfment and clearance of ACs and DAMPs to mitigate inflammation and restore homeostasis [14]. After engulfing and recycling ACs and DAMPs, phagocytes facilitate the resolution of inflammation by secreting anti-inflammatory cytokines while inhibiting the release of pro-inflammatory cytokines [15–17]. Therefore, targeting efferocytosis in modulating inflammatory responses and facilitating tissue repair represents a promising strategy following SAH.

In addition to “eat-me” signals, ACs also express “don’t eat-me” signals to inhibit efferocytosis, such as CD47. CD47 interacts with SIRP α on phagocytes to prevent their engulfment [18]. Signal regulatory protein alpha (SIRP α), also known as CD172a, was initially identified as a membrane protein predominantly present on

macrophages and myeloid cells. SIRP α is characterized by three immunoglobulin-like domains, a single transmembrane region, and a cytoplasmic domain that contains four tyrosine residues with immunoreceptor tyrosine-based inhibitory motifs (ITIMs) [19]. During apoptosis, CD47 on apoptotic cells similarly engages with SIRP α , resulting in the phosphorylation of SIRP α ’s four tyrosine residues on the cytoplasmic domain and subsequent recruitment and activation of Src homology region 2 (SH2) domain-containing phosphatases, specifically SHP1 and SHP2, which inhibit efferocytosis [20, 21]. The loss of myeloid cell-specific SIRP α , but not CD47, diminishes inflammation and suppresses atherosclerosis [22]. In nonalcoholic steatohepatitis (NASH), blockade of the CD47-SIRP α axis enhances necroptotic hepatocyte clearance by liver macrophages and reduces hepatic fibrosis [23]. Additionally, blockade of this axis accelerates hematoma clearance and alleviates neuroinflammation following intracerebral hemorrhage [24, 25]. SIRP α deficiency has been shown to accelerate pathological processes in models of Parkinson’s disease [26]. Our preliminary study indicated that SIRP α levels are aberrantly elevated in the cerebrospinal fluid of patients with SAH and are significantly correlated with patient prognosis. These findings suggest that SIRP α may serve as a promising target for the regulation of inflammation and efferocytosis.

This study aims to investigate the precise role and mechanisms of efferocytosis mediated by SIRP α . Our findings demonstrate that SIRP α levels are aberrantly elevated following SAH. Knockdown of SIRP α in microglia promotes efferocytosis and mitigates neuroinflammation in both in vivo and in vitro models, mediated by the dephosphorylation of key transcription factors of “eat-me” signals, specifically STAT6, by SHP1. Targeting the CD47-SIRP α -SHP1 axis holds significant potential for the development of neuroprotective therapies.

Materials and methods

Ethics statement

The study protocol was approved by the Ethics Committee of Nanjing Jinling Hospital, Affiliated Hospital of Medical School, Nanjing University and was conducted in accordance with the principles of Good Clinical Practice and the Declaration of Helsinki. All patients signed an informed consent form. All animal procedures were approved by the Animal Care and Use Committee of Nanjing University and were performed in accordance with institutional guidelines.

SAH patients and CSF sample

The SAH patients’ inclusion criteria were as follows: (1) written informed consent from either the patient or a family member; (2) age ≥ 18 and ≤ 70 years; and (3) diagnosis of subarachnoid hemorrhage by computed

tomography (CT scan). Aneurysms were verified through digital subtraction angiography (DSA). Exclusion criteria included: (1) Patients with a history of CNS diseases (e.g., stroke, traumatic brain injury, CNS infection) or accompanied by serious comorbidities before SAH onset (e.g., severe coagulation disorders, malignant tumor, uncontrollable heart disease, and hypertension) or other organ dysfunctions within 6 months; (2) non-aneurysmal SAH (e.g., trauma, arteriovenous malformation, and angiogram-negative SAH). All CSF samples of the control group were obtained from intraspinal anesthesia before surgery in patients with non-neurological diseases. This research included 40 SAH patients admitted to Nanjing Jinling Hospital within 1 day of their SAH onset and the CSF sample was obtained by lumbar puncture. All patients received standard medical care after admission and the Hunt-Hess Grade was used to evaluate patient prognosis. The samples were centrifuged at 3000 rpm for 10 min at 4 °C to remove cells (erythrocytes and immune cells) and stored at -80 °C until analysis.

4D label-free quantitative proteome and analysis

Proteomics was conducted to explore the variation in protein content in CSF of SAH patients and was carried out at Allwegene Co., Ltd (Beijing, China). Protein extraction and trypsin digestion were conducted, followed by LC-MS/MS. The MaxQuant search engine (1.5.3.17) was used for MS/MS data analysis. FDR was adjusted to $\leq 1\%$.

ELISA

Commercial kits were utilized to quantify concentrations of IL-1 β (ABclonal, RK00001), IL-18 (ABclonal, RK00176) and SIRP α (FineTest, EH3784) in the Human CSF according to the manufacturer's instructions. Commercial kits were utilized to quantify concentrations of IL-1 β (ABclonal, RK00006), IL-18 (ABclonal, RK00104), IL-10 (ABclonal, RK00016) and TGF- β 1 (ABclonal, RK00057) in the culture medium according to the manufacturer's instructions. Absorption at 450 nm was determined using a microplate reader (Thermo Scientific) and the IL-1 β , IL-18, SIRP α , IL-10, TGF- β 1 concentration was determined according to the standard curve generated at the same time.

Primary neuron culture

Primary cortical neurons were prepared from the cortex of fetal (E16–18) C57BL/6J mice with a modified method as previously described [27]. In brief, the fetal mice were decapitated and placed in 75% alcohol for sterilizing. The brain was separated in HBSS (Thermo Fisher Scientific, Waltham, MA, USA) with the aid of a dissection microscope. After the leptomeninges and white matter were carefully removed, the cortex was digested in 0.125%

trypsin for 15 min at 37 °C in a humidified atmosphere of 5% CO₂ and 95% air. Then, 20% FBS was added to the brain tissue suspension to terminate digestion and the brain tissue suspensions were passed through a 40 μ m filter and centrifuged at 1000 r/min for 5 min. The cell pellets were re-suspended in Dulbecco's modified Eagle's medium (DMEM, Thermo Fisher Scientific, Waltham, MA, USA) with 20% Fetal Bovine Serum (FBS, Thermo Fisher Scientific, Waltham, MA, USA) and penicillin-streptomycin (Thermo Fisher Scientific, Waltham, MA, USA). After that, the suspensions were seeded into poly-D-lysine-coated plates. Two hours later, the culture medium was replaced with Neurobasal Medium (Thermo Fisher Scientific, Waltham, MA, USA) containing Gluta-MAX-I (Thermo Fisher Scientific, Waltham, MA, USA), B27 supplement (Thermo Fisher Scientific, Waltham, MA, USA) and penicillin-streptomycin. Cultures were maintained at 37 °C in a humidified atmosphere of 5% CO₂ and 95% air. Subsequently, half of the medium was replaced every 2 days.

Primary microglia culture

Cells were dissociated from the cortex of fetal (E16–18) C57BL/6J mice, plated on flasks, and cultivated in DMEM supplemented with 10% FBS and 1% penicillin-streptomycin at 37 °C in a humidified atmosphere of 5% CO₂ and 95% air. After 12–14 d of culture, mature microglia were separated from mixed glial cultures by quick and gentle shaking, resuspended in DMEM supplemented with 10% FBS and penicillin-streptomycin, and plated onto plates. Cultures were maintained at 37 °C in a humidified atmosphere of 5% CO₂ and 95% air. Subsequently, the medium was replaced every 2 days.

SAH model

In *in vivo* experiments, the experimental SAH model was achieved by pre-chiasmatic injection of autologous blood according to a previous study [28]. Male C57BL/6J mice (8–10 weeks old, GemPharmatech Co., Ltd, Nanjing, China) were placed under general anesthesia with 2% isoflurane in 100% O₂ and maintained with 1% isoflurane. After induction of anesthesia, the head was fixed in a stereotactic apparatus. With a midline incision, the skin overlying the anterior skull was opened. A burr hole was drilled into the skull 4.5 mm anterior to the bregma with a caudal angle of 40° using a 0.9-mm drill. Blood (60 μ L) was withdrawn from a C57BL/6 WT blood donor and injected over a 10-second period with a 29-gauge needle advanced through the burr hole at a 40° angle until reaching the base of the skull. The needle was kept in this position for 5 min to prevent backflow or CSF leakage. After the injection, the burr hole was plugged immediately with bone wax. Sham treated controls received the same procedure with injection of physiologic saline.

In *in vitro* experiments, OxyHb (Millipore Sigma, Burlington, MA, USA) was prepared and resolved into 20 μM with culture medium and sterilized by filtration through a 0.22-μm sterile filter. Neurons and microglia were stimulated with 10 μM OxyHb to mimic SAH condition as determined in a prior study.

Adeno-associated virus delivery *in vivo*

SIRPα knockdown of microglia *in vivo* specifically was achieved by AAV transfection which was designed and synthesized by Genechem Co., Ltd (Shanghai, China). The SIRPα RNAi sequence is 5'-CCTCCGGATCAAACAGAAGAA-3', and the scrambled NC sequence is 5'-TCTCCGAACGTGTCACGT-3'. The shRNA was ligated into the pAAV-CD68p-EGFP-MIR155(MCS)-WPRE-SV40 PolyA GV684 plasmid. The expressing plasmid was co-transfected with pHelper (carrying adenoviral origin genes) and pAAV-RC (carrying AAV replication and capsid genes) plasmids into AAV-293 cells for packaging AAV9 particles. The shRNA-SIRPα AAV particles have a titer of 1.62×10^{13} v.g./mL determined by real-time PCR. In *in vivo* experiments, mice were anesthetized and placed in a stereotaxic frame. A total of 5 μL of the AAV-NC, AAV-SIRPα was injected into the lateral ventricles at a rate of 0.3 μL/min. The SAH model was established 30 days after the AAV injection.

Transfections and RNA interference, site mutant

Transfection was achieved using jetPRIME® transfection reagent (Polyplus, 101000046) according to the manufacturer's protocol. All plasmids were constructed by GeneChem Co. Ltd (Shanghai, China) and verified by sequencing. After 24 h to 48 h incubation, the transfection mixture was removed and replaced with a fresh complete medium. The plasmid vector expressing short hairpin RNA (shRNA) targeting the sequence of SIRPα gene (CCTCCGGATCAAACAGAAGAA), STAT6 gene (GGCTTTCCGGAGTCACTATAA) and negative control (TTCTCCGAACGTGTCACGT) were synthesized and cloned into GV684 vector (purchased from Shanghai Genechem Co., Ltd.), recombinant vector was detected by DNA sequencing. The final products were then transfected into *Escherichia coli*. DH5α followed by extraction with Endofree plasmid Mega kit (Qiagen, Hilden, Germany) obtained shRNA-SIRPα and shRNA-STAT6 plasmid.

Mouse SIRPα NM_001291019.2(Y440/464/481/505 A) was obtained from the cDNA library of Genechem (Shanghai, China) with the following primers: SIRPα forward: 5'-GAGGATCCCCGGGTACCGGTCGCCACCA TGCTTCTGGCCATGGTC-3' and reverse: 5'-CACAC ATTCCACAGGCTAGTCATATCTTGCCCTCCTCATCC CTCTCATC-3'. The vector plasmid CV702 and SIRPα_{mut} gene sequence were digested by BamHI and HindIII

restriction enzymes, and complete cloning through the In-fusion recombination method. The recombinant vector was detected by DNA sequencing. The final products were then transfected into *Escherichia coli*. DH5α followed by extraction with Endofree plasmid Mega kit (Qiagen, Hilden, Germany) obtained SIRPα_{mut} overexpression plasmid.

Western blot

The total protein and surface membrane protein samples were extracted from brain tissues of C57BL/6J mice or primary cultured neurons and microglia for immunoblotting analysis. For the total protein, the brain sample of mice was removed rapidly after saline perfusion and rinsed in 0.9% normal saline (4 °C) to wash away the blood and blood clots. The samples were lysed in radioimmunoprecipitation assay buffer (Beyotime, Nantong, China) containing 1% protease and phosphatase inhibitor cocktails (Beyotime, Nantong, China). The homogenate after ultrasonic lysis was then centrifuged at $12,000 \times g$ for 15 min and supernatants (containing cytosolic and membrane fractions) were collected. Total protein concentrations were measured with the BCA Protein Assay Kit (Beyotime, Nantong, China). Equal amounts of protein were separated by 7.5-12.5% SDS-PAGE (EpiZyme, Shanghai, China) and PVDF membrane (Millipore Sigma, Burlington, MA, USA). The membrane was blocked with 5% defatted milk for 2 h at room temperature then incubated overnight at 4 °C with primary antibodies against SIRPα (1:1000, ABclonal, A9001), CD47(1:1000, ABclonal, A21904), SHP1 (1:1000, Abcam, ab227503), SHP2(1:1000, Abcam, ab300579), PY20 (1:1000, Biologend, 309301), p-SHP1 (1:1000, Cell Signaling Technology, 8849), p-SHP2 (1:1000, ABclonal, AP0267), STAT6 (1:1000, ABclonal, A19120), p-STAT6(1:1000, Cell Signaling Technology, 56554), CD36(1:1000, ABclonal, A19016), MerTK (1:1000, Abcam, ab300136), IL-1β(1:1000, ABclonal, A22257), IL-18(1:1000, ABclonal, A23076), TGF-β1 (1:1000, ABclonal, A21244), IL-10 (1:1000, ABclonal, A12255), Bax (1:1000, ABclonal, A19684), Bcl-2 (1:1000, ABclonal, A19693), Cleaved Caspase-3 (1:1000, Cell Signaling Technology, 9664), Flag (1:1000, ABclonal, AE063), β-actin (1:2000, ABclonal, AC038), GAPDH(1:2000, ABclonal, A19056) in primary antibody dilution buffer (Servicebio, Wuhan, China). After the membrane was washed for 10 min each of three times in TBST, the membrane was incubated in the appropriate HRP-conjugated secondary antibody (1:5000, ABclonal) in secondary antibody dilution buffer (Servicebio, Wuhan, China) for 2 h at room temperature. The blotted protein bands were visualized by enhanced chemiluminescence (ECL) western blot detection reagents (MilliporeSigma, Burlington, MA, USA). ImageJ software

version 1.54f (National Institutes of Health, Bethesda, MD, USA) quantified band intensities.

Immunofluorescence staining

Immunofluorescence staining was performed as previously described [29]. Briefly, frozen brain Sect. (8 μm) and cultured cells on coverslips were fixed in 4% paraformaldehyde, respectively. Following treatment with 0.3% Triton X-100, the samples were blocked with Immunol Staining Blocking Buffer (Beyotime, Shanghai, China) for 60 min. These samples were incubated with specific primary antibodies for NeuN (1:400, Cell Signaling Technology, 24307), Iba1(1:100, Abcam, ab283319), MAP2 (1:200, ABclonal, A22206) in Universal Antibody Diluent (New Cell & Molecular, Suzhou, China) at 4 °C overnight. Then, the samples were slowly washed three times with phosphate-buffered saline with 0.5% Tween-20 (PBST) and incubated with corresponding secondary antibodies (Alexa Fluor 488/555, 1:200, Thermo Fisher Scientific, Waltham, MA, USA) for 2 h at room temperature (RT). After washing 3 times with PBST, the samples were counterstained with 4,6-diamidino-2-phenylindole (DAPI, MilliporeSigma, 1:2000) for 10 min at RT. Fluorescence was visualized by a fluorescence microscope (Leica, THUNDER Imaging Systems, Germany).

Nissl staining

Tissue sections were stained with cresyl violet (Nissl) (Beyotime, Shanghai, China). Nissl staining was performed to evaluate neuronal survival after SAH. Brain Sect. (8 μm) were hydrated in 1% toluidine blue for 10 min. After washing with double distilled water, they were dehydrated and mounted with Permount. Normal neurons have relatively big cell bodies, rich in cytoplasm, with one or two big round nuclei, whereas damaged cells have shrunken cell bodies, condensed nuclei, dark cytoplasm, and numerous empty vesicles.

TUNEL assay

TUNEL staining was performed according to the manufacturer's instructions (E-CK-A320, Elabscience, Wuhan, China). Brain sections were incubated with primary antibody against NeuN at 4 °C overnight. Following washing with PBST, the slides

were sequentially incubated with a TUNEL reaction mixture for 1 h at 37 °C. After washing again, the slides were counterstained with DAPI for 10 min. The positive cells were identified, counted, and analyzed by two investigators blinded to the grouping.

Efferocytosis assay

Efferocytosis assay was performed as previously described [30]. In *in vitro* experiments, approximately 5×10^5 microglia were seeded in a 24-well plate,

exposed to experimental SAH stimuli and incubated with CMFDA (HY-126561, MedChemExpress)-labeled apoptotic neurons at a ratio of 1:5 at 37 °C for 30 min. The cells were collected and resuspended and blocked with Fc block antibody (BD, Biosciences) for 20 min at room temperature. Then, anti-Iba1 (1:200, Abcam, ab178846) and ABflo[®] 647-conjugated Goat anti-Mouse IgG (H+L) (1:100, ABclonal, AS059) were added to the cells and stained for 30 min at room temperature in the dark. The proportion of microglia that exhibited increased fluorescence (corresponding to phagocytosis of fluorescent-labeled apoptotic cells) was determined by flow cytometry on a NovoCyte™ flow cytometer (ACEA Biosciences) or by a fluorescence microscope (Leica, THUNDER Imaging Systems, Germany). For fluorescent observation, at least three images per well were captured for the efferocytosis assay. To inhibit the phagocytic activity of microglia, the cells were pretreated with 10 μM Cytochalasin D (C8273, Sigma-Aldrich) for 1 h and then washed before incubated with CMFDA-labeled apoptotic neurons.

Neuron-microglia cocultures

Neuron-microglia cocultures were performed as previously described [31]. 10 μM Hb was added in ten-day-old neurons cultured in a 24-well plate (3×10^5 /well) for 12 h. Primary microglia (7.5×10^4 /well) were then seeded and cultured together with neurons for 12 h in a co-culture medium (250 μL neural basal medium and 250 μL DMEM/F12-based glia cell medium). To inhibit the phagocytic activity of microglia, the cells were pretreated with 10 μM Cytochalasin D (C8273, Sigma-Aldrich) for 1 h and then washed before coculturing.

Behavioral testing

The method of the Morris water maze test has been previously described [32]. The test was conducted in a circular tank with a diameter of 180 cm and a depth of 50 cm. A circular platform, measuring 12 cm in diameter, was positioned 2 cm below the water surface. All mice underwent training for 4 consecutive days, starting on the 18th day post-modeling, with three trials per day. Each trial lasted for 1 min, with a 5-minute intertrial interval. If the mice successfully located the platform within 1 min, it was allowed to remain on the platform for 15 s. If the mice failed to find the platform within the time limit, it was gently guided to the platform. The testing phase occurred from the 22nd to the 26th day post-SAH.

RNA isolation and quantitative real-time polymerase chain reaction (qRT-PCR)

Total RNA was extracted from both cultured cells and tissue utilizing the RNA isolater Total RNA Extraction Reagent (Vazyme, Nanjing, China) according to the

manufacturer's instructions. A NanoDrop 2000 spectrophotometer (Thermo Fisher Scientific, USA) was subsequently used to accurately determine the concentration of total RNA in each sample. Afterward, the RNA samples were converted into cDNA through reverse transcription using the HiScript[®]III RT SuperMix for qPCR along with gDNA wiper (Vazyme, Nanjing, China). RT-qPCR was subsequently conducted using the Mx3000/Mx3005P real-time PCR system (Agilent, USA) and Taq Pro Universal SYBR[®] qPCR Master Mix (Vazyme, China). The mRNA expression was normalized to β -actin and GAPDH, and the relative expression was quantified using the $2^{-\Delta\Delta C_t}$ method. The primers were synthesized (Generay Biotech, Shanghai, China) using the sequences shown in Table 1.

Co-IP

Co-IP was performed according to the manufacturer's instructions (88804, Thermo Fisher Scientific, Waltham, MA, USA). Total protein was extracted from brain tissues of C57BL/6J mice and cultured microglia utilizing a comprehensive lysis buffer mixture. Following centrifugation at $12,000 \times g$ for 15 min at 4 °C, the protein concentration in the supernatant was measured using a BCA kit. A total of 500 μ g of protein was incubated with with control IgG (AC005, ABclonal), anti-SIRP α (144001, Biolegend, USA) and anti-STAT6 (5397, Cell Signaling Technology) at 4 °C overnight with constant rotation. The samples were subsequently combined with magnetic protein beads for 2 h at RT. Finally, the protein bound to the beads was eluted and analyzed by Western blot.

RNA-seq and analysis

The RNA-seq and analysis was carried out at Genechem Co., Ltd (Shanghai, China). The RNA of cells was first extracted (SIRP α _mut versus Ctrl; $n = 3$ each). After quality control of RNA, the Illumina RNA libraries were constructed with the NEBNext Ultra RNA Library Prep Kit. The RNA library was sequenced by the Illumina NovaSeq platform, and then 150-base pair paired-end reads were

produced. In-house Perl scripts were used to process all raw data of fastq format, and then the clean data were acquired with strict quality control. The Hisat2 was chosen as a mapping tool to construct the database of splice junctions following the gene model annotation file.

A differential expression analysis of cells (SIRP α _mut versus Ctrl; $n = 3$ each) was performed using the DESeq2 R package (1.16.1). For controlling the false discovery rate, Benjamini and Hochberg's approach was performed to adjust the resulting P values. The genes with an adjusted P value less than 0.05 tested by DESeq2 were considered differentially expressed. GO/KEGG enrichment analysis based on the differentially expressed genes was performed by the clusterProfiler R package. GO/KEGG terms with adjusted P value < 0.05 were assigned as significantly enriched by differentially expressed genes.

Chromatin Immunoprecipitation (ChIP) assay

The microglia were fixed using formaldehyde (F809702, Macklin) after the corresponding treatment. ChIP assay was performed using a Sonication ChIP Kit (RK20258, ABclonal). The prepared chromatin-protein complexes were immunoprecipitated using protein A/G magnetic beads (RM02915, ABclonal) coated with anti-p-STAT6 antibody (#56554T, Cell Signaling Technology) or anti-IgG antibody (RM20712, ABclonal). DNA was released from the chromatin-protein complex and purified using AFTSpin Multifunction DNA Purification Kit (RK30100, ABclonal). Diluted DNA was further subjected to PCR using primers and quantified using agarose gel electrophoresis, followed by staining with Ultra GelRed (GR501, Vazyme).

Luciferase reporter assays

The putative or mutated promoter regions of MerTK and CD36 were synthesized by Genechem (Shanghai, China) and the fragments were digested by NheI and HindIII restriction endonucleases. Then they were cloned into the pGL3-basic plasmid. The luciferase reporter plasmid containing the putative or mutated promoter region of MerTK and CD36 and the pRL-TK reporter plasmid (cDNA encoding Renilla luciferase) were co-transfected into the microglia. After 24–48 h, microglia were stimulated with 10 μ M OxyHb and co-cultured with apoptotic neurons at a 1:5 ratio. After 12 h, the cells were lysed, and luciferase activity was determined using the Dual Luciferase Reporter Gene Assay Kit (11402ES60, YEASEN) according to the manufacturer's protocols. All plasmids were purchased from GeneChem Co. Ltd (Shanghai, China).

Statistical analysis

The data were demonstrated as means \pm SEM and analyzed with GraphPad Prism software (version 10.0), of

Table 1 Primers for quantitative real-time polymerase chain reaction (qRT-PCR)

Targets	Primers
SIRP α -MOUSE-F	GGCTCCTGGTGAATGTATCTGC
SIRP α -MOUSE-R	GTGTTCTCAGCGCGGTATT
MerTK-promoter-MOUSE-F	GGTCACTCCAGGTGCTAGAT
MerTK-promoter-MOUSE-R	GGAATGAAGCACTGGCCATTTTA
CD36-promoter-MOUSE-F	GCCTGACAGCCATTGACATC
CD36-promoter-MOUSE-R	ACTGAGGCACAAAATGAGGGT
ACTB-MOUSE-F	CGCAGCGATATCGTCATCCA
ACTB-MOUSE-R	TCCTTTGTCCCCTGAGCTTG
GAPDH-MOUSE-F	TTCGCACCAGCATCCCTAGA
GAPDH-MOUSE-R	GTGCAGTGCCAGGTGAAAAT

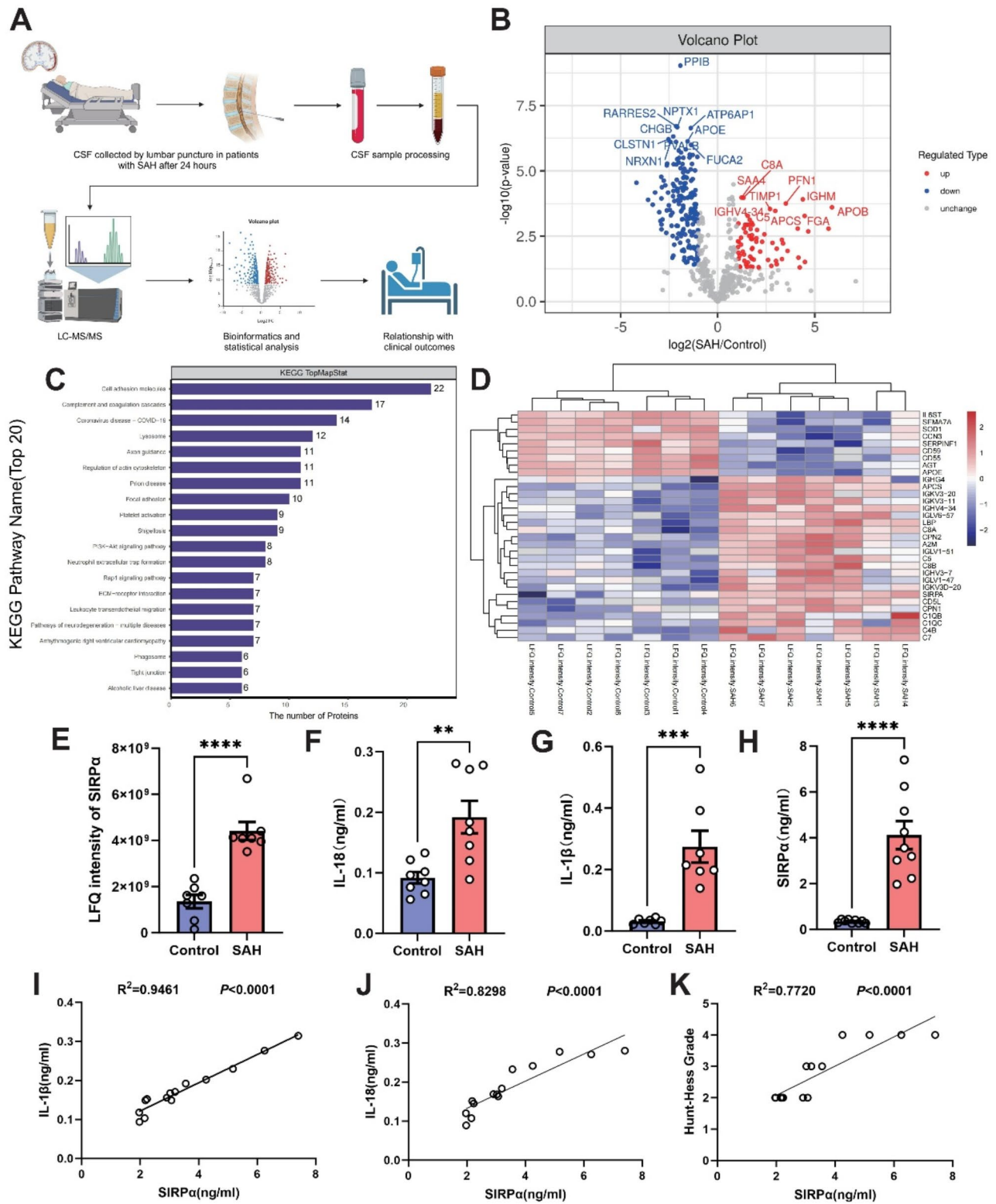


Fig. 1 (See legend on next page.)

(See figure on previous page.)

Fig. 1 SIRP α levels are elevated in CSF of patients with SAH and associated with prognosis. **(A)** Schematic diagram of lumbar puncture for CSF collection and proteomic analysis. **(B)** Volcano plot of upregulated proteins and downregulated proteins in CSF of patients with SAH. X-axis: log₂ ratio of protein levels between CSF of patients with SAH and healthy control. Y-axis: the p-value (-log₁₀ transformed) of proteins, fulfilling the criteria |log₂ (fold change)| ≥ 1 and $P < 0.05$ ($n = 7$ each group). **(C)** KEGG enrichment analysis of differential protein levels between CSF of patients with SAH and healthy control, fulfilling the criteria |log₂ (fold change)| ≥ 1 and $P < 0.05$ ($n = 7$ each group). **(D)** Heatmap representing differential protein levels in the “Regulation of Inflammatory Response” pathway from GO enrichment analysis, fulfilling the criteria |log₂ (fold change)| ≥ 1 and $P < 0.05$ ($n = 7$ each group). **(E)** LFQ intensity of SIRP α protein levels in the CSF of SAH patients and healthy controls ($n = 7$ each group). **(F)** IL-18 levels in the CSF of SAH patients compared to healthy controls ($n = 8$ each group). **(G)** IL-1 β levels in the CSF of SAH patients compared to healthy controls ($n = 7$ each group). **(H)** SIRP α levels in the CSF of SAH patients compared to healthy controls ($n = 9$ each group). **(I)** Simple linear regression analysis between SIRP α and IL-1 β levels in SAH patients ($n = 14$ each group). **(J)** Simple linear regression analysis between SIRP α and IL-18 levels in SAH patients ($n = 14$ each group). **(K)** Simple linear regression analysis between SIRP α levels and Hunt-Hess grade in SAH patients ($n = 14$ each group). All values are means \pm SEM, * $P < 0.05$, ** $P < 0.01$, *** $P < 0.001$, **** $P < 0.0001$, ns, no significant changes

which the $P < 0.05$ was considered significant. The data were obtained from the results of at least three independent experiments. A t-test was utilized to analyze the differences between groups. And one-way analysis of variance or two-way analysis of variance (ANOVA) test with Tukey’s post hoc test was utilized for assessing the differences in mean values of more than two groups.

Results

SIRP α levels are elevated in CSF of patients with SAH and correlate with prognosis

The metabolites present in CSF can provide an accurate representation of changes in the microenvironment of the CNS, offering valuable insights for the treatment of CNS diseases [33]. To identify differential protein levels in the CSF of patients with SAH compared to healthy controls, a 4D label-free quantitative proteomic analysis was performed (Fig. 1A). Principal component analysis (PCA) revealed a distinct separation between the CSF of patients with SAH and that of healthy controls (Fig. S1). The proteomic analysis revealed 69 upregulated proteins and 174 downregulated proteins (Fig. 1B). KEGG enrichment analysis indicated that these differential proteins are significantly enriched in pathways related to “Lysosome”, “Regulation of cytoskeleton”, and “Phagosome” all of which are components of efferocytosis (Fig. 1C). GO enrichment analysis further highlighted that these proteins are involved in the “Regulation of inflammatory response”, with a heatmap analysis of this pathway revealing that SIRP α was markedly elevated in the CSF of SAH patients (Fig. 1D-E). After conducting proteomic analysis, we assessed the levels of SIRP α , IL-1 β , and IL-18 in the CSF of patients with SAH using ELISA. The results demonstrated a significant increase in the levels of SIRP α , IL-1 β , and IL-18 in the CSF of SAH patients (Fig. 1F-H). Moreover, SIRP α levels were found to be positively correlated with the Hunt-Hess grade, a key prognostic indicator in SAH patients (Fig. 1I). Additionally, a positive correlation was observed between SIRP α and the levels of IL-1 β and IL-18 in the CSF, suggesting an association between SIRP α and the inflammatory response in SAH (Fig. 1J-K). Taken together, these findings support the

potential role of SIRP α as both a biomarker for inflammation and a prognostic indicator in SAH patients. Furthermore, SIRP α -induced efferocytosis may represent a novel therapeutic target for mitigating EBI following SAH.

Knockdown of SIRP α enhances efferocytosis by microglia and mitigates neuroinflammation following SAH in vivo

To explore the role of SIRP α in modulating efferocytosis and neuroinflammation after SAH, we generated SIRP α knockdown microglia using adeno-associated viruses (AAVs) with a CD68 (microglia-specific marker)-specific promoter and EGFP tags. Immunofluorescence assays confirmed efficient gene knockdown (Fig. S2). WB analysis was conducted to assess the expression levels of SIRP α and CD47 over different time points following SAH. SIRP α expression was low in the sham group but significantly elevated in the experimental groups, peaking at 24 h and gradually diminishing by 72 h post-SAH. In contrast, the expression of CD47, the ligand for SIRP α , did not exhibit significant changes (Fig. 2A-B). RT-qPCR further corroborated these findings, showing a similar temporal pattern of SIRP α expression (Fig. 2C). Co-IP assays were performed in vivo using SIRP α as the target protein to assess the interaction between CD47 and SIRP α . The results demonstrated that CD47 established interaction with SIRP α following SAH and the levels of CD47/SIRP α did not exhibit significant alterations (Fig. S3). Subsequently, immunofluorescence and three-dimensional imaging were employed to evaluate the extent of efferocytosis. The percentage of phagocytic microglia (Neun(red)⁺Iba1(green)⁺ cells) was significantly higher in the SAH+AAV-SIRP α group compared to the SAH+AAV-NC group, indicating that efferocytosis was enhanced following specific knockdown of SIRP α in microglia (Fig. 2D-E). WB analysis was performed to assess the expression levels of inflammatory cytokines IL-1 β , IL-18, IL-10, and TGF- β 1, as well as apoptosis-related proteins Bax, Bcl-2, and cleaved caspase-3. In the SAH+AAV-SIRP α group, the expression levels of the pro-inflammatory cytokines IL-1 β and IL-18 were significantly reduced, while the levels of the anti-inflammatory cytokines IL-10 and TGF- β 1 were notably increased

when compared to the SAH+AAV-NC group. Additionally, the expression of cleaved caspase-3 was reduced, and the ratio of Bcl-2/Bax was elevated in the SAH+AAV-SIRP α group compared to the SAH+AAV-NC group (Fig. 2F-G).

Morphological and fractal analyses revealed that, following SAH stimulation, microglia exhibited pronounced retraction, a shortened, less branched morphology, and an increase in size, indicating a significant polarization toward a reactive phenotype. These morphological changes were notably mitigated by the knockdown of microglial SIRP α (Fig. 2H-I). To evaluate long-term neurological outcomes, Morris water maze (MWM) tests were performed between days 22 and 26 post-SAH to assess the impact of microglial SIRP α knockdown on cognitive function. The results from the training trial showed no significant differences in escape latency or swimming distance among the experimental groups. However, the MWM test revealed that microglial SIRP α knockdown significantly reduced both the escape latency to the platform and the total swimming distance (Fig. 2J-K). TUNEL staining further demonstrated a significant reduction in the number of TUNEL-positive neurons after SAH when microglial SIRP α was knocked down (Fig. 2L). Nissl staining also showed that, although the temporal cortical neurons were substantially damaged following SAH, this damage was largely reversed upon microglial SIRP α knockdown (Fig. 2M). These findings suggest that microglial SIRP α knockdown may promote efferocytosis, alleviate neuroinflammation and confer sustained neuroprotective effects following SAH.

Knockdown of SIRP α enhances efferocytosis by microglia and mitigates neuroinflammation following SAH in vitro

In the CNS, SIRP α is expressed in both neurons and microglia, but its expression is minimally detectable in astrocytes and oligodendrocytes [26]. To investigate the changes in SIRP α expression following SAH in vitro, neurons and microglia were stimulated with 10 μ M OxyHb, a classical in vitro model for SAH. WB analysis was performed to assess SIRP α expression at various time points following SAH. In microglia, SIRP α expression was low in the sham group but significantly elevated in the experimental groups, peaking at 12 h post-SAH and gradually decreasing by 48 h. In contrast, SIRP α expression in neurons did not show significant changes over the time course (Fig. 3A-B). To explore the role of SIRP α in modulating efferocytosis and neuroinflammation after SAH in vitro, we constructed microglia with SIRP α knockdown efficiencies of 70% and 90%, respectively, through the transfection of plasmids. WB assays confirmed efficient gene knockdown (Fig. S4A-B). To further explore the role of SIRP α in efferocytosis and neuroinflammation following SAH in vitro, microglia were stimulated with 10 μ M

OxyHb and co-cultured with Green CMFDA-labeled apoptotic neurons at a 1:5 ratio, where the apoptotic neurons were induced by 20 μ M OxyHb. This co-culture system was used to mimic efferocytosis and the SAH condition simultaneously. Flow cytometry and immunofluorescence analyses revealed that the number of Green CMFDA⁺Iba1⁺ cells, a marker for efferocytosis, was significantly increased in the Hb+ACs+shSIRP α -70 and Hb+ACs+shSIRP α -90 group, compared to the Hb+ACs+shCtrl group. This effect was inhibited by pre-treatment of microglia with 10 μ M Cytochalasin D (an inhibitor of actin polymerization and efferocytosis) for 1 h (Fig. 3C-F). Subsequently, microglia were stimulated with OxyHb and co-cultured with non-labeled apoptotic neurons at a 1:5 ratio. And lysosomal activity was assessed using the lysosomal acidity probe LysoSensor, which serves as an indicator of lysosomal activity. The fluorescence intensity in the Hb+ACs+shSIRP α -70 and Hb+ACs+shSIRP α -90 groups were significantly higher compared to the Hb+ACs+shCtrl group, indicating enhanced lysosomal activity. This increase was also inhibited by Cytochalasin D pre-treatment of microglia (Fig. 3G-H). To assess the inflammatory response in vitro, the culture medium from the co-culture system was collected, and the levels of extracellular cytokines were measured using ELISA. The results showed that in the Hb+ACs+shSIRP α -70 and Hb+ACs+shSIRP α -90 group, the levels of the pro-inflammatory cytokines IL-1 β and IL-18 were significantly reduced, while the levels of the anti-inflammatory cytokines IL-10 and TGF- β 1 were significantly elevated, compared to the Hb+ACs+shCtrl group (Fig. 3I). Next, we investigated whether SIRP α is essential for microglia-mediated neuronal protection as previously described [31]. Neurons were exposed to 10 μ M OxyHb for 12 h, after which microglia were co-cultured with the OxyHb-treated neurons for an additional 12 h (Fig. 3J). Consistent with our previous findings, the number of surviving neurons was significantly higher in the Hb+ACs+shSIRP α -70 and Hb+ACs+shSIRP α -90 group compared to the Hb+ACs+shCtrl group (Fig. 3K-L). Through these experiments, we found that SIRP α knockdown enhances efferocytosis and mitigates neuroinflammation following SAH in vitro, although the precise mechanisms underlying these effects require further investigation.

Contribution of the unilateral signal of SIRP α to the efferocytosis by microglia and neuroinflammation following SAH in vitro

To investigate the intracellular mechanisms underlying SIRP α -mediated efferocytosis in microglia and neuroinflammation following SAH, Co-IP assays were performed in microglia with stimulation of 10 μ M OxyHb and ACs using SIRP α as the target protein to assess the interaction

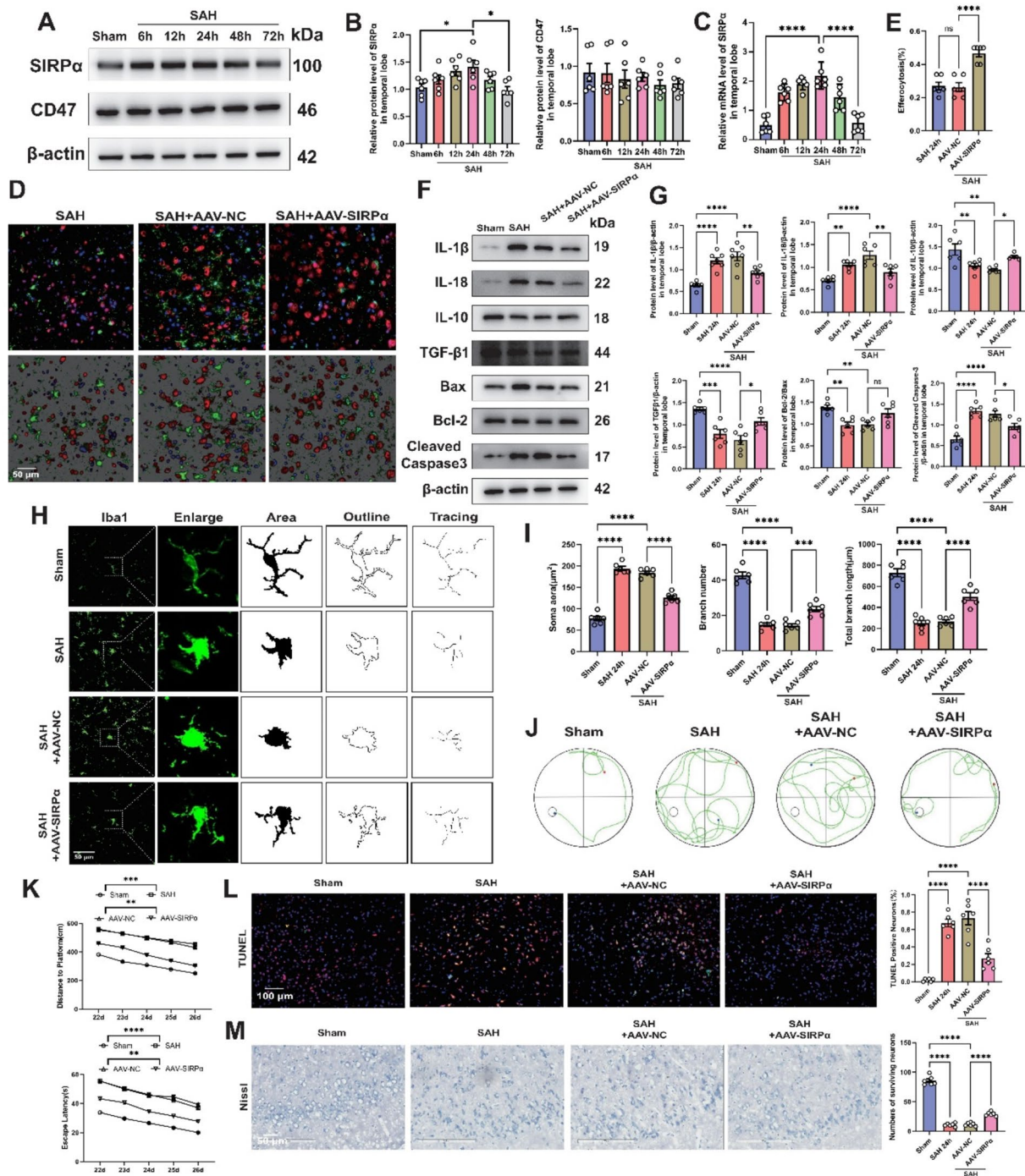


Fig. 2 Knockdown of SIRPα enhances efferocytosis by microglia and mitigates neuroinflammation following SAH in vivo. **A**. Western blot assay for the expression of SIRPα and CD47 in the temporal lobe after SAH. **B**. Quantification of SIRPα and CD47 protein levels ($n=6$ each group). **C**. RT-qPCR for SIRPα in the temporal lobe after SAH ($n=6$ each group). **D**. Representative immunofluorescence images and three-dimensional imaging showing the extent of efferocytosis following SAH for 24 h. White arrowheads indicate dead/dying neurons that were engulfed by microglia (Neun(red)⁺Iba1(green)⁺). Scale bar, 50 μm. **E**. Quantification of efferocytosis levels (Neun(red)⁺Iba1(green)⁺ microglia) following SAH for 24 h ($n=6$ each group). **F**. Western blot assay for the expression of IL-1β, IL-18, IL-10, TGF-β1, Bax, Bcl-2 and Cleaved caspase-3 in all groups in the temporal lobe following SAH after knockdown of SIRPα. **G**. Quantification of IL-1β, IL-18, IL-10, TGF-β1, Bax, Bcl-2 and Cleaved caspase-3 protein levels in the temporal lobe following SAH after knockdown of SIRPα. **H**. Skeletonized analysis: Representative images of microglia. Scale bar, 50 μm. **I**. Quantification of soma area, branch numbers, and total branch length ($n=6$ each group). **J-K**. Representative swimming tracks of the mice in all groups of the MWM tests and quantitative analyses of latency and distance. **L**. Representative fluorescent images and quantification of TUNEL+ neurons following SAH for 24 h. Nuclei were counterstained with DAPI (blue), ($n=6$ each group). Scale bar, 100 μm. **M**. Representative Nissl staining images of the temporal lobe in all groups ($n=6$ each group). Scale bar, 50 μm. All values are means ± SEM, * $P < 0.05$, ** $P < 0.01$, *** $P < 0.001$, **** $P < 0.0001$, ns, no significant changes

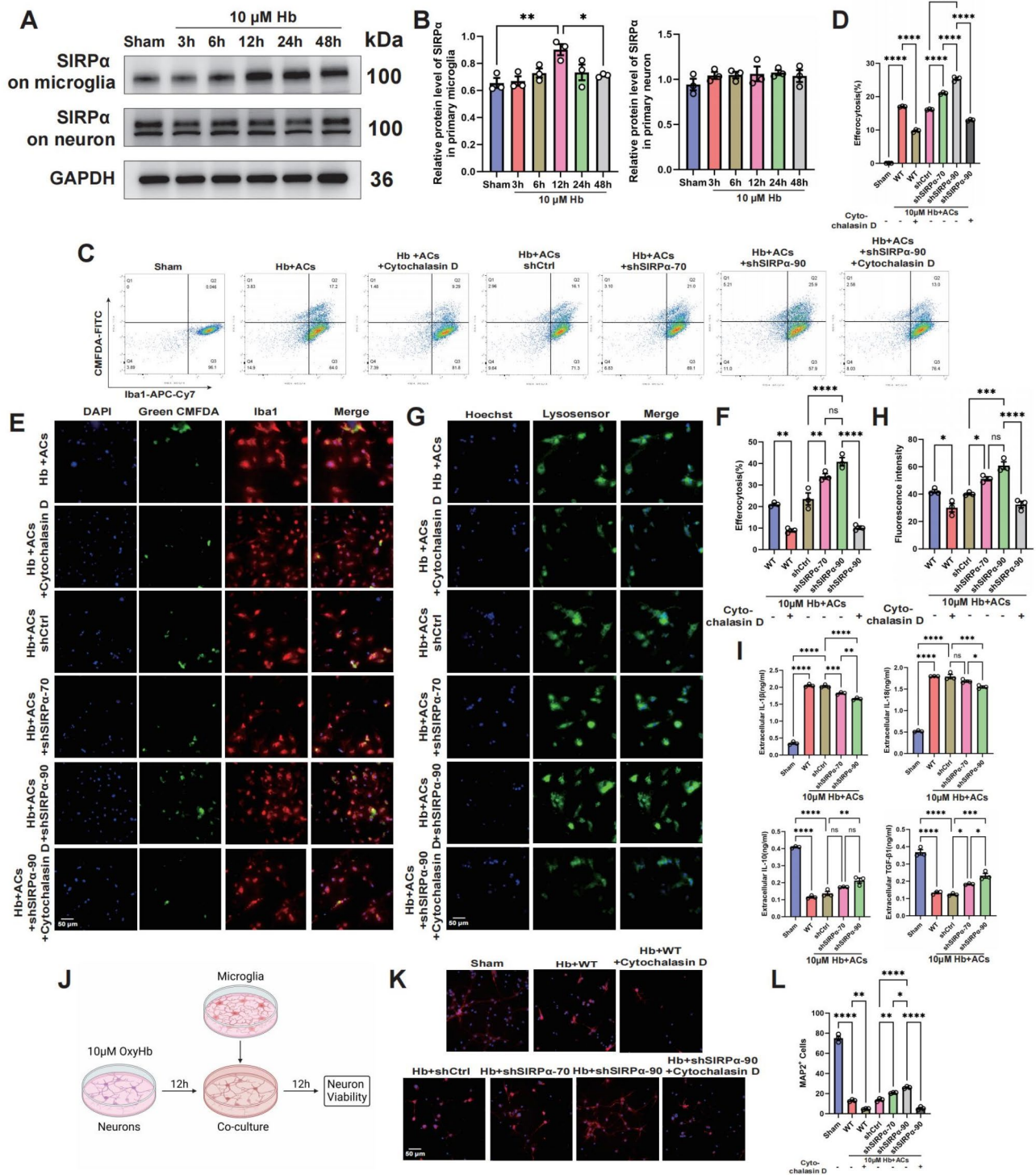


Fig. 3 (See legend on next page.)

between SHP1, SHP2 and SIRP α . In the sham group, the expression levels of SIRP α and p-SHP1 were low, whereas in the experimental groups, both were significantly upregulated, peaking at 12 h post-SAH and gradually declining by 48 h. Similarly, the expression of p-SHP2

was also low in the sham group but showed a marked increase in the experimental groups, reaching its highest levels at 6 h post-SAH, with a subsequent decrease observed by 48 h (Fig. 4A-D). The results demonstrated that SIRP α recruits and phosphorylates both SHP1 and

(See figure on previous page.)

Fig. 3 Knockdown of SIRP α enhances efferocytosis by microglia and mitigates neuroinflammation following SAH in vitro. **(A)** Western blot assay for the expression of SIRP α in primary microglia and neurons after 10 μ M Hb stimulation. **(B)** Quantification of SIRP α protein levels in microglia and neurons ($n=3$ each group). **C-D.** Flow cytometry analysis and quantification of CMFDA⁺Iba1⁺ microglia ($n=3$ each group). **E.** Representative immunofluorescence images of CMFDA (green) and Iba1 (red) in microglia after 10 μ M Hb and ACs stimulation for 12 h. Nuclei were counterstained with DAPI (blue). Scale bar, 50 μ m. **F.** Quantification of CMFDA⁺Iba1⁺ microglia numbers ($n=3$ each group). **G.** Representative immunofluorescence images of Lysosensor (green) in microglia after 10 μ M Hb and ACs stimulation for 12 h. Live cells were counterstained with Hoechst (blue). Scale bar, 50 μ m. **H.** Quantification of fluorescence intensity of Lysosensor ($n=3$ each group). **I.** The levels of IL-1 β , IL-18, IL-10 and TGF- β 1 in culture medium from the co-culture system ($n=3$ each group). **J.** Experimental design. Primary neurons were subjected to 12 h 10 μ M Hb stimulation and then co-cultured with WT, shCtrl and shSIRP α microglia for 12 h. Neuronal survival was measured 24 h later by MAP2 staining. **K.** Representative images of MAP2-stained neurons after co-cultured with WT, shCtrl and shSIRP α microglia. Scale bar, 50 μ m. **L.** Quantification of the number of MAP2⁺ (red) neurons ($n=3$ each group). All values are means \pm SEM, * $P < 0.05$, ** $P < 0.01$, *** $P < 0.001$, **** $P < 0.0001$, ns, no significant changes

SHP2 following SAH in vitro. WB analysis was conducted to assess the expression levels of SHP1 and SHP2, as well as their phosphorylation status, at various time points following SAH. In the sham group, the levels of p-SHP1/SHP1 and p-SHP2/SHP2 were low. In contrast, these levels were significantly upregulated in the experimental groups, p-SHP1/SHP1 were peaking at 12 h post-SAH and gradually decreasing by 48 h but the levels of p-SHP2/SHP2 were peaking at 6 h (Fig. 4A, E-F). Based on the immunoblot analysis of p-SHP1, which demonstrated a more pronounced signal and a time course similar to that of SIRP α , whereas p-SHP2 exhibited a distinct time course in both IP and Input, we propose that SIRP α primarily recruits and phosphorylates SHP1. Consequently, we focused on investigating the downstream mechanisms by targeting SHP1 in subsequent experiments.

Subsequently, we mutated the tyrosine residues at positions 440, 464, 481, and 505 in the intracellular region of SIRP α to alanine, a non-phosphorylatable amino acid. To investigate the role of SIRP α mutations in modulating efferocytosis and neuroinflammation following SAH in vitro, we generated SIRP α _mut microglia through plasmid transfection with FLAG tags. Western blot (WB) analysis confirmed the successful induction of gene mutations (Fig. S4C). Co-IP assays were performed in microglia using SIRP α as the target protein to investigate the recruitment and phosphorylation of SHP1. The results demonstrated that the recruitment and phosphorylation of SHP1 by SIRP α were significantly reduced following mutation of the intracellular tyrosine residues (Fig. 4G-H). Immunofluorescence and flow cytometry analyses revealed a significant increase in the number of Green CMFDA⁺Iba1⁺ cells in the Hb + ACs + SIRP α _mut group compared to the Hb + ACs + Ctrl group. This effect was also inhibited by pre-treatment of microglia with 10 μ M Cytochalasin D for 1 h (Fig. 5A-D). Additionally, the fluorescence intensity of Lysosensor in the Hb + ACs + SIRP α _mut group was markedly higher than in the Hb + ACs + Ctrl group, suggesting enhanced lysosomal activity. This increased fluorescence intensity was also suppressed by Cytochalasin D pre-treatment of microglia (Fig. 5E-F). ELISA analysis in the culture

medium showed that, in the Hb + ACs + SIRP α _mut group, levels of the pro-inflammatory cytokines IL-1 β and IL-18 were significantly reduced, while the levels of the anti-inflammatory cytokines IL-10 and TGF- β 1 were significantly elevated, relative to the Hb + ACs + Ctrl group (Fig. 5G). Consistent with our previous method, the number of surviving neurons was significantly greater in the Hb + ACs + SIRP α _mut group compared to the Hb + ACs + Ctrl group in the co-culture system (Fig. 5H-I). These findings underscore the critical role of SHP1 and SHP2 recruitment and phosphorylation by the intracellular domain of SIRP α in regulating efferocytosis and neuroinflammation following SAH in vitro.

Mutation of the intracellular domain of SIRP α enhances the expression of MerTK and CD36

To identify the downstream regulators involved in SIRP α -mediated efferocytosis and neuroinflammation, we performed RNA-seq on microglia stimulated with 10 μ M OxyHb and ACs, with or without mutations at tyrosine residues 440, 464, 481, and 505 in the intracellular domain of SIRP α , substituting them with alanine. PCA revealed a clear separation between the SIRP α _mut group compared to the Ctrl group. (Fig. S6). The Venn diagram (Fig. 6A) illustrates that 11,025 genes are expressed in both groups. The volcano plot (Fig. 6B) reveals 789 upregulated genes and 950 downregulated genes in the SIRP α _mut group compared to the Ctrl group. GO enrichment analysis indicated that these differentially expressed genes are predominantly involved in the “inflammatory response” (Fig. 6C). Furthermore, we selected the top 100 genes associated with “phagocytosis” and “efferocytosis” from GeneCards for heatmap analysis (Fig. 6D-E). Notably, the results showed that *Mertk* and *Cd36*, both of which function as “eat-me” signals, were significantly upregulated (Fig. 6F-G). WB analysis also confirmed that MerTK and CD36 were significantly upregulated (Fig. 6H-J). In the sham group, CD36 expression was low, but it was significantly elevated in the experimental groups, peaking at 6 h post-SAH and gradually decreasing by 48 h in vitro. In contrast, MerTK did not exhibit significant changes (Fig. 6K-M). Collectively, mutations at tyrosine residues 440, 464, 481, and 505 in

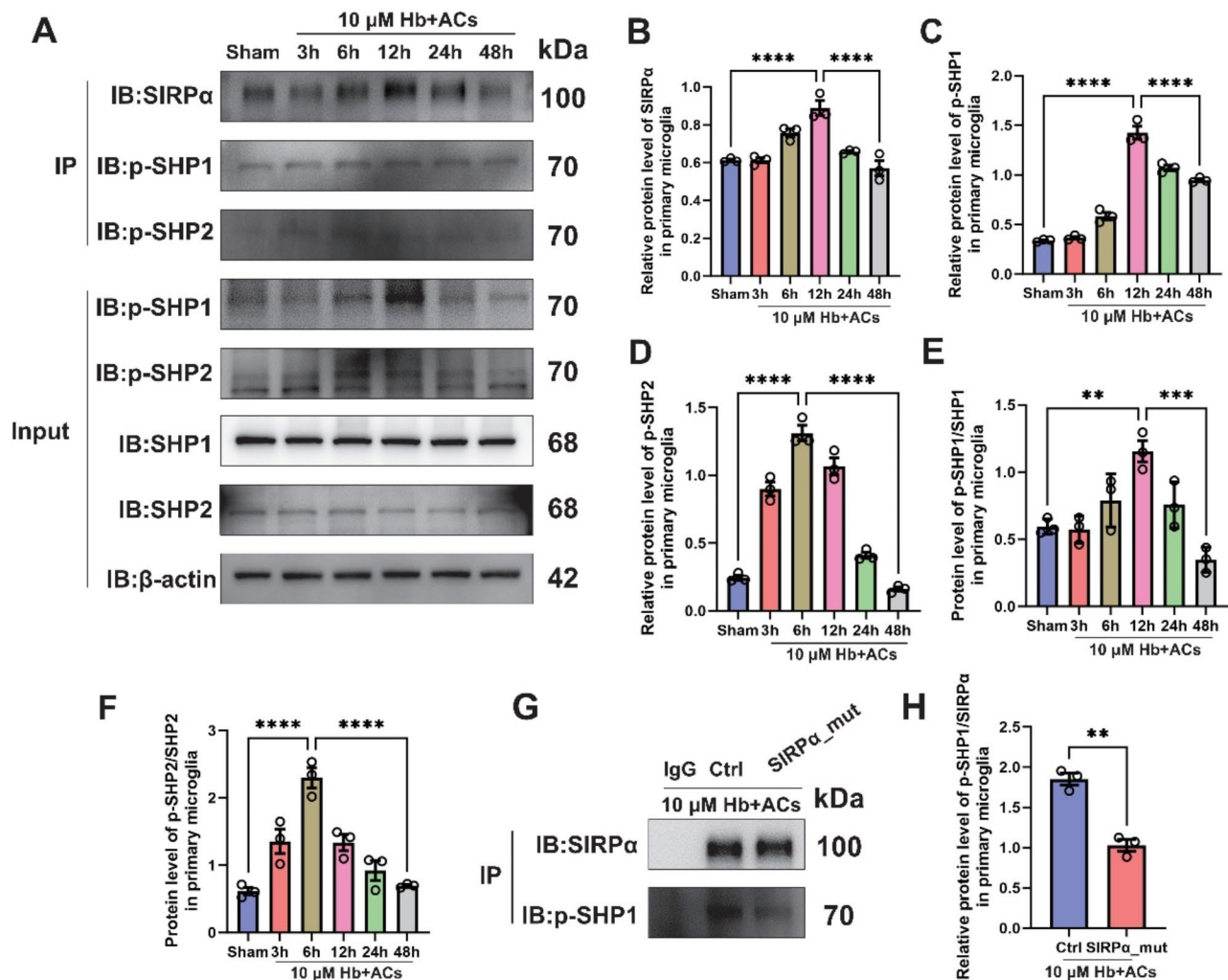


Fig. 4 SHP1 and SHP2 recruitment and phosphorylation by the intracellular domain of SIRP α in regulating efferocytosis following SAH in vitro. **A.** Association between SIRP α , SHP-1, and SHP-2 was assessed by Western blot analysis after the co-immunoprecipitation (Co-IP) of SIRP α in microglia after 10 μ M Hb and ACs stimulation. **B-D.** Quantification of SIRP α , and p-SHP1, p-SHP2 protein levels interacted with SIRP α ($n=3$ each group). **E-F.** Quantification of p-SHP1/SHP1 and p-SHP2/SHP2 protein levels ($n=3$ each group). **G.** Association between SIRP α and SHP-1 was assessed by Western blot analysis after the Co-IP of SIRP α in Ctrl and SIRP α _mut microglia after 10 μ M Hb and ACs stimulation. **H.** Quantification of p-SHP1 protein levels interacted with SIRP α ($n=3$ each group). All values are means \pm SEM, * $P < 0.05$, ** $P < 0.01$, *** $P < 0.001$, **** $P < 0.0001$, ns, no significant changes

the intracellular domain of SIRP α enhance the expression of MerTK and CD36, both of which act as “eat-me” signals to promote efferocytosis.

STAT6 is a common transcription factor of *Mertk* and *Cd36* and is dephosphorylated by SHP1 following SAH

To investigate the mechanism by which SIRP α regulates *Mertk* and *Cd36*, we performed bioinformatics analyses using the UCSC Genome Browser (<http://genome.ucsc.edu/index.html>) and JASPAR (<https://jaspar.elixir.no/>), an open-access database of curated and non-redundant transcription factor binding profiles. These analyses suggested that STAT6 may serve as a common transcription factor directly regulating the expression of MerTK and CD36. The binding motif is shown in Fig. 7A. A

5'-AAGGGTTCAT-3' motif in the promoter region of the *Mertk* and A 5'-AAGAGACATT-3' motif in the promoter region of the *Cd36* are predicted to be STAT6 binding sites (Fig. 7B-C). RNA-seq and WB analysis further confirmed that STAT6 was significantly upregulated (Fig. 7D-F). In the sham group, p-STAT6 expression was low, but it was significantly elevated in the experimental groups, peaking at 12 h post-SAH and gradually decreasing by 48 h in vitro. STAT6 itself did not exhibit significant changes, and the p-STAT6/STAT6 ratio followed a similar trend to that of p-STAT6 (Fig. 7G-J). To verify the binding of p-STAT6 to the promoter regions of *Mertk* and *Cd36*, a chromatin immunoprecipitation (ChIP) assay was conducted. Compared to the IgG control group, the p-STAT6 group showed a significant increase in relative

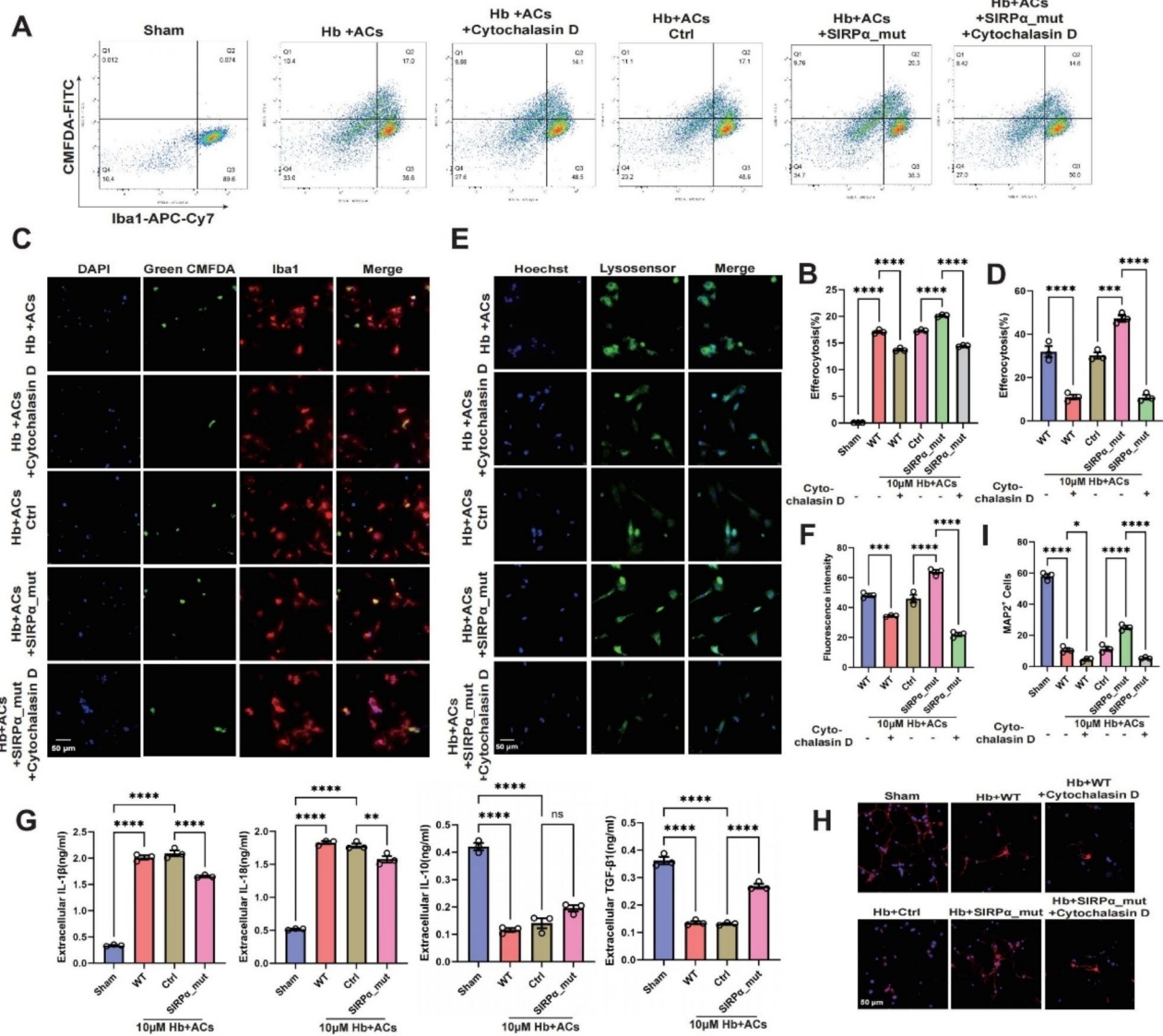


Fig. 5 Mutation of the intracellular domain of SIRPα enhances efferocytosis by microglia and mitigates neuroinflammation following SAH in vitro **A-B.** Flow cytometry analysis and quantification of CMFDA⁺Iba1⁺ microglia ($n=3$ each group). **C.** Representative immunofluorescence images of CMFDA (green) and Iba1 (red) in microglia after 10μM Hb and ACs stimulation for 12 h. Nuclei were counterstained with DAPI (blue). Scale bar, 50 μm. **D.** Quantification of CMFDA⁺Iba1⁺ microglia numbers ($n=3$ each group). **E.** Representative immunofluorescence images of Lysosensor (green) in microglia after 10μM Hb and ACs stimulation for 12 h. Live cells were counterstained with Hoechst (blue). Scale bar, 50 μm. **F.** Quantification of fluorescence intensity of Lysosensor ($n=3$ each group). **G.** The levels of IL-1β, IL-18, IL-10 and TGF-β1 in culture medium from the co-culture system ($n=3$ each group). **H.** Representative images of MAP2-stained neurons after co-cultured with microglia. Scale bar, 50 μm. **I.** Quantification of the number of MAP2⁺ neurons ($n=3$ each group). All values are means ± SEM, * $P < 0.05$, ** $P < 0.01$, *** $P < 0.001$, **** $P < 0.0001$, ns, no significant changes

enrichment in the Input (Fig. 7K-M). To investigate the binding site of p-STAT6 to the promoter regions of *Mertk* and *Cd36*, the luciferase reporter assays were performed and we mutated the 5'-AAGGGTTCAT-3' motif to 5'-GGCCTCGGAA-3 in the promoter region of *Mertk*, and the 5'-AAGAGACATT-3' motif to 5'-GGCCTCGGAA-3' in the promoter region of *Cd36*. The luciferase reporter assays revealed that site-directed mutagenesis could abolish the decreased promoter activity in STAT6-knockdown microglia (Fig. 7N-O). Subsequently, Co-IP

assays were conducted using STAT6 as the target protein to assess the interaction between SHP1 and STAT6. The expression level of p-STAT6 was significantly increased in the SIRPα_mut group compared to the Ctrl group (Fig. 9P, R). And the expression level of p-SHP1 was significantly decreased in the SIRPα_mut group compared to the Ctrl group (Fig. 7P-Q). The above data indicated that the dephosphorylation of p-STAT6 by SHP1 was reduced following mutations at tyrosine residues 440, 464, 481, and 505 in the intracellular domain of SIRPα.

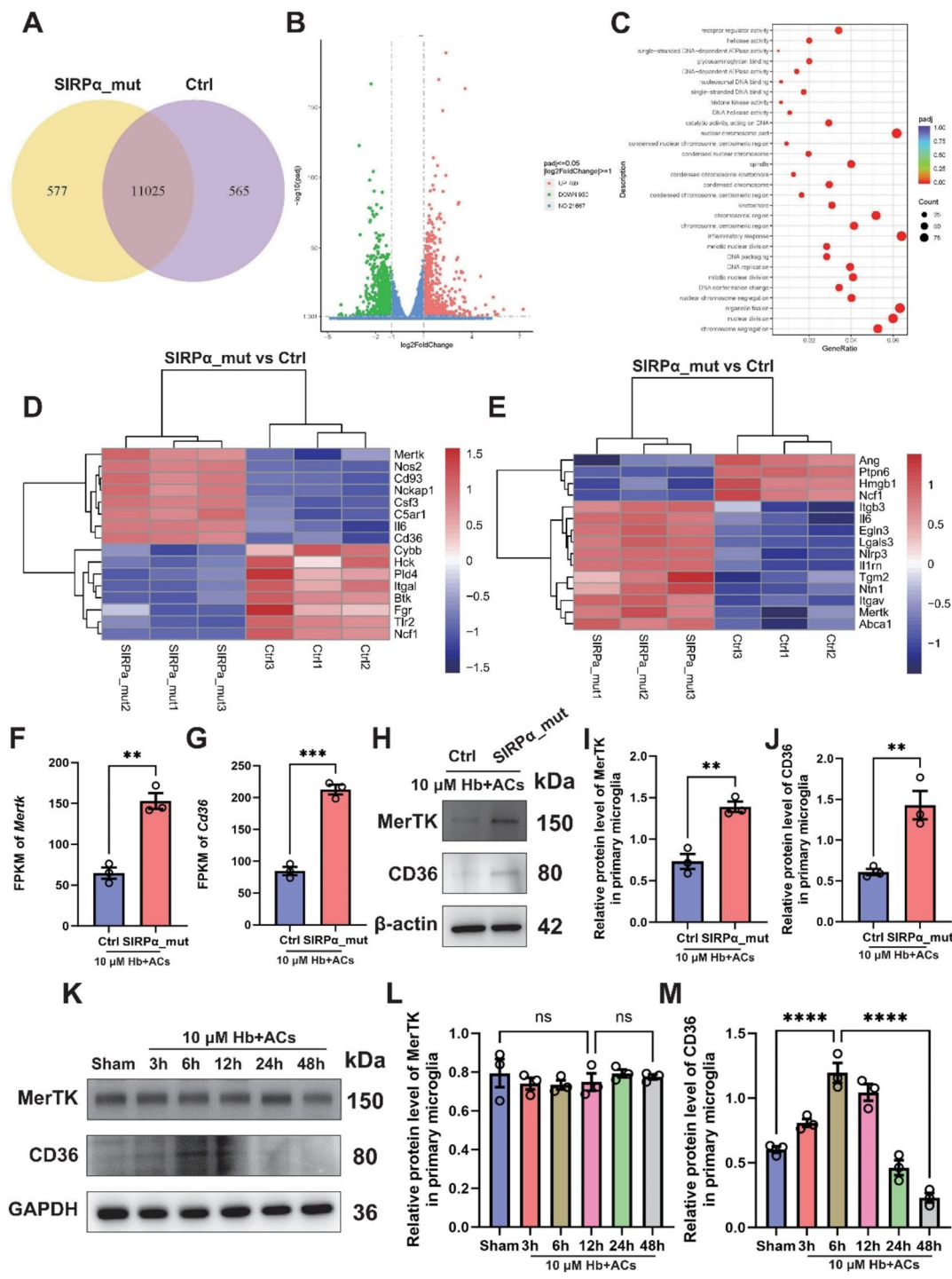


Fig. 6 Mutation of the intracellular domain of SIRPα enhances the expression of MerTK and CD36. **(A)** The Venn diagram illustrates that 11,025 genes are expressed in both groups. **(B)** Volcano plot of differentially expressed genes (DEGs) in microglia following mutation of the intracellular domain of SIRPα. X-axis: log₂ ratio of differentially expressed genes between SIRPα_{mut} and Ctrl. Y-axis: the p-value (-log₁₀ transformed) of proteins, fulfilling the criteria |log₂ (fold change)| ≥ 1 and P < 0.05 (n = 7 each group). **(C)** GO enrichment analysis of DEGs between SIRPα_{mut} and Ctrl, fulfilling the criteria |log₂ (fold change)| ≥ 1 and P < 0.05 (n = 7 each group). **(D)** Heatmap analysis of co-expressed genes in DEGs and the top 100 phagocytosis-related genes identified by GeneCards. **(E)** Heatmap analysis of co-expressed genes in DEGs and the top 100 efferocytosis-related genes identified by GeneCards. **F-G.** Expression of MerTK and Cd36 in microglia from RNA-seq results (n = 3 each group). **H.** Western blot assay for the expression of MerTK and CD36 protein levels in microglia following mutation of the intracellular domain of SIRPα. **I-J.** Quantification of MerTK and CD36 protein levels (n = 3 each group). **K.** Western blot assay for the expression of MerTK and CD36 in primary microglia after 10 μM Hb and ACs stimulation. **L-M.** Quantification of MerTK and CD36 protein levels (n = 3 each group). All values are means ± SEM, *P < 0.05, **P < 0.01, ***P < 0.001, ****P < 0.0001, ns, no significant changes

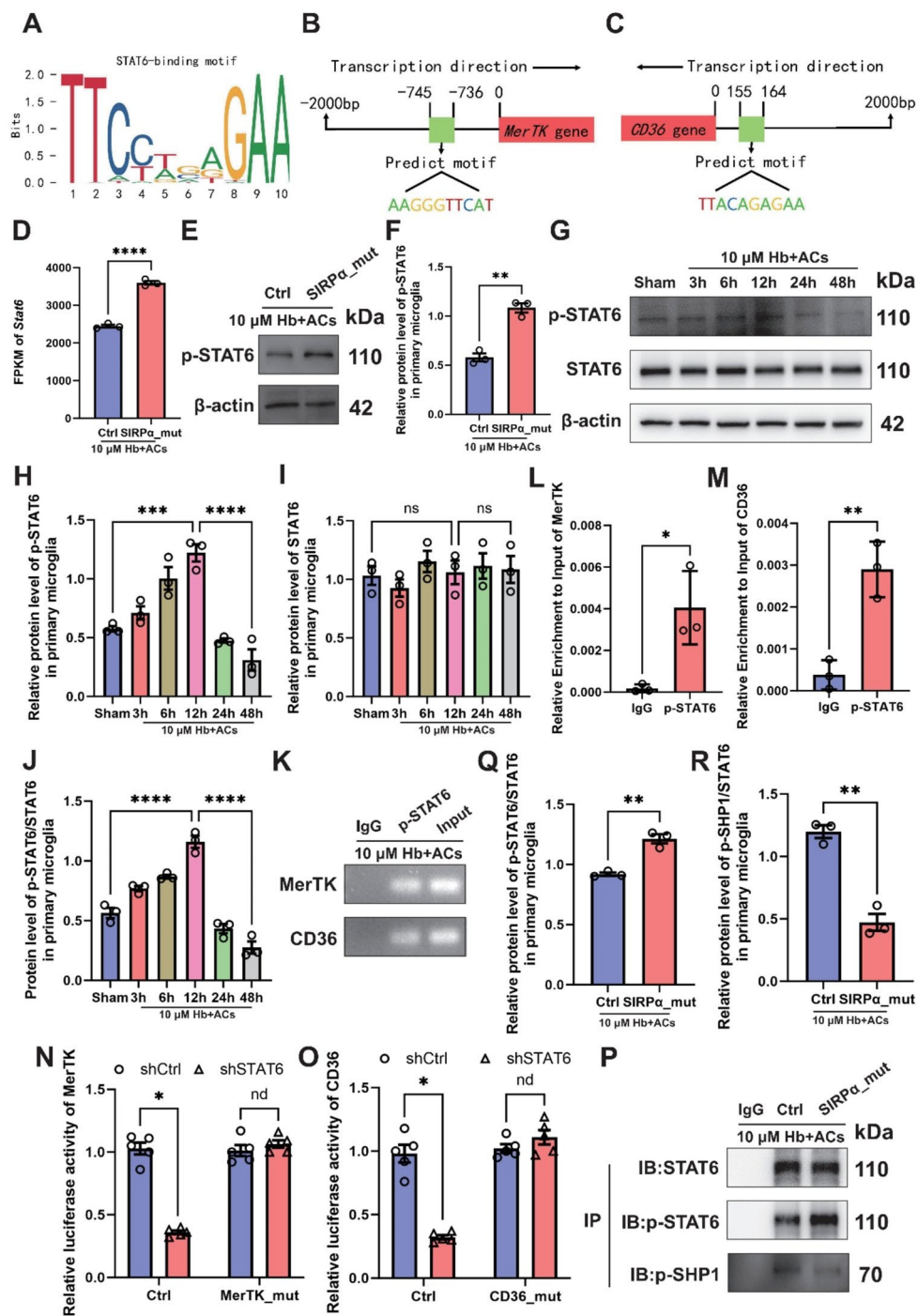


Fig. 7 STAT6 is a common transcription factor of MerTK and CD36 and is dephosphorylated by SHP1 following SAH. **A-C**. Potential STAT6-binding site in the promoter region of the MerTK and CD36. **D**. Expression of Stat6 in microglia from RNA-seq results ($n=3$ each group). **E**. Western blot assay for the expression of p-STAT6 in microglia following mutation of the intracellular domain of SIRPα. **F**. Quantification of p-STAT6 protein levels ($n=3$ each group). **G**. Western blot assay for the expression of p-STAT6 and STAT6 in primary microglia after 10 μM Hb and ACs stimulation. **H-J**. Quantification of p-STAT6, STAT6 and p-STAT6/STAT6 protein levels ($n=3$ each group). **K-M**. Representative agarose gel electrophoresis images and quantification for PCR products of ChIP assay ($n=3$ each group). **N-O**. Quantification of luciferase activity of MerTK and CD36 in Ctrl, MerTK_mut and CD36_mut microglia with or without STAT6-knockdown ($n=3$ each group). **P**. Association between STAT6 and SHP-1 was assessed by Western blot analysis after the Co-IP of STAT6 in Ctrl and SIRPα_mut microglia after 10 μM Hb and ACs stimulation. **Q**. Quantification of p-SHP1 and p-STAT6 protein levels interacted with STAT6 ($n=3$ each group). All values are means ± SEM, * $P < 0.05$, ** $P < 0.01$, *** $P < 0.001$, **** $P < 0.0001$, ns, no significant changes

Moreover, STAT6 functions as a common transcription factor for *Mertk* and *Cd36* following SAH in vitro.

Discussion

In this study, our pivotal discoveries are as follows: [] (1) SIRP α levels are significantly elevated in the CSF of patients with SAH and are correlated with clinical prognosis []. (2) SAH enhances the expression of SIRP α in microglia; both in vivo and in vitro knockdown of SIRP α promotes efferocytosis, thereby reducing neuroinflammation and EBI []. (3) SIRP α recruits and phosphorylates SHP1 and SHP2 through four tyrosine residues in its cytoplasmic domain, thereby inhibiting efferocytosis following SAH, with SHP1 playing a particularly significant role []. (4) Phosphorylated SHP1 dephosphorylates STAT6, a transcription factor that plays a crucial role in regulating the expression of “eat-me” signals, such as MerTK and CD36, thereby inhibiting efferocytosis. A schematic representation of this mechanism is illustrated in Fig. 8.

The prevailing view is that CSF is produced via two primary pathways: the choroid plexus system and the brain parenchyma system, with the choroid plexus responsible for approximately 80% of total CSF production. CSF is continuously produced and absorbed into the venous system, functioning similarly to lymphatic fluid within the CNS [34]. It provides essential nutrients to brain cells, facilitates the transport of metabolites from brain tissues, regulates the acid-base balance of the CNS, and buffers pressure on the brain and spinal cord, thus offering protective and supportive functions. With advancements in protein sequencing technology, numerous studies have identified biomarkers such as tau, SOD1, and PARK7 that are strongly correlated with disease prognosis through protein sequencing analysis of CSF from patients with Alzheimer’s disease and Parkinson’s disease [35, 36]. This has significantly aided in the diagnosis and treatment of these conditions. Consequently, the metabolites present in CSF can accurately reflect changes in the brain’s microenvironment and offer valuable insights for the treatment of CNS diseases [33].

Previous studies have indicated that efferocytosis plays a pivotal role in tissue repair and homeostasis. Upon tissue injury, phagocytes are recruited to the site of damage where they engulf and clear dying cells through efferocytosis [37]. Efferocytosis suppresses the secretion of pro-inflammatory cytokines, stimulates the production of anti-inflammatory cytokines, modulates the phenotype of microglia and macrophages, accelerates the resolution of inflammation, and promotes tissue repair [38, 39]. It involves three main stages: recognition, engulfment, and degradation of dying cells. Key molecules in efferocytosis, such as “find-me” signals, “eat-me” signals, and “don’t

eat-me” signals, have been shown to modulate efferocytosis following injury [40].

We therefore conducted a proteomic analysis of CSF from patients with SAH. Our results indicated a significant increase in SIRP α levels in CSF collected 24 h post-onset of SAH, with proteins exhibiting significant differences enriched in pathways related to efferocytosis and inflammation. Subsequently, ELISA results revealed that levels of SIRP α , IL-1 β , and IL-18 were significantly elevated. Notably, SIRP α levels demonstrated a significant correlation with both IL-1 β and IL-18, as well as the Hunt-Hess grade of patients. These findings underscore the critical role of efferocytosis and SIRP α in mitigating EBI following SAH. After that, we observed a concomitant increase in SIRP α expression in both in vivo and in vitro models of SAH. Following the knockdown of SIRP α in microglia, we noted a significant enhancement in efferocytosis and a reduction in neuroinflammation. In vivo, immunofluorescence staining revealed a substantial increase in the phagocytic index, and microglia exhibited a more ramified morphology, characterized by an increase in branching and a decrease in cell size, suggesting a shift toward a steadier state. Additionally, we observed a reduction in the pro-inflammatory cytokines IL-1 β and IL-18, and an elevation in the anti-inflammatory cytokines IL-10 and TGF- β 1 following SIRP α knockdown in microglia. Furthermore, TUNEL and Nissl staining indicated a reduction in neuronal damage. Moreover, SIRP α knockdown in microglia improved long-term outcomes in Morris water maze tests after SAH. To assess efferocytosis in vitro, we co-cultured microglia with CMFDA-labeled apoptotic neurons, induced by 20 μ M Hb, at a 1:5 ratio. Following the SIRP α knockdown, the number of CMFDA⁺ microglia was significantly increased. Additionally, we employed Lyso-sensor to measure lysosomal acidity, which serves as an indicator of lysosomal digestive activity. Results showed that lysosomal activation and acidity were enhanced following SIRP α knockdown. Furthermore, when apoptotic neurons (induced by 10 μ M Hb) were co-cultured with SIRP α -deficient microglia at a 5:1 ratio, there was a significant increase in the survival of neurons following SIRP α knockdown.

SIRP α is involved in controlling inflammatory response as well as efferocytosis in microglia and macrophages [41, 42]. SIRP α is a myeloid-expressed immunoreceptor that contains tyrosine-based inhibitory motifs (ITIMs). Its canonical function, through interaction with the self-recognition marker CD47, is to inhibit the activity of professional phagocytes [43]. Under various stimulatory conditions, the ITIMs of SIRP α become phosphorylated, leading to the recruitment and phosphorylation of Src homology 2 (SH2) domain-containing tyrosine phosphatases SHP1 and SHP2 [21, 44]. SHP1/2 are non-receptor

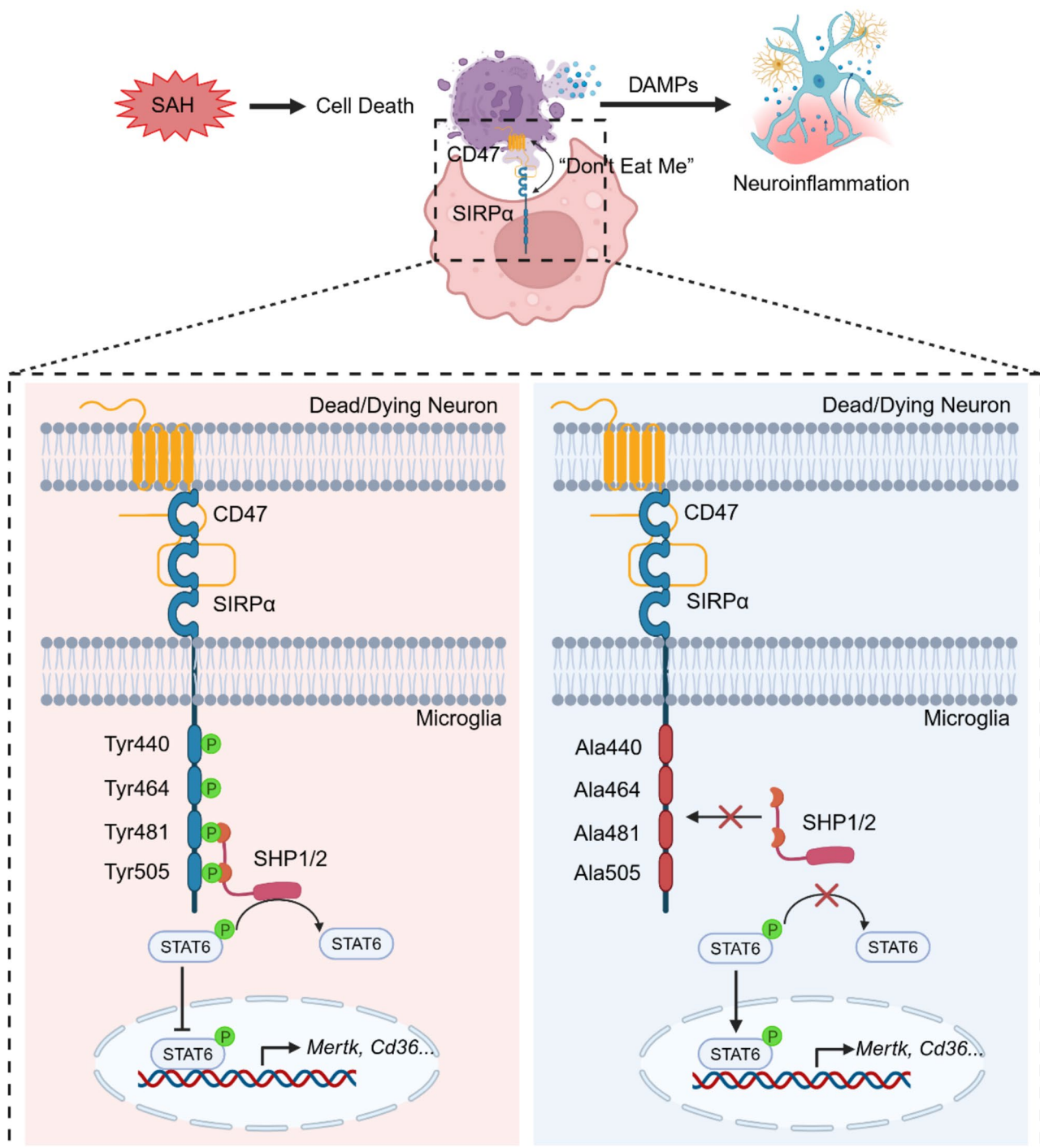


Fig. 8 SIRPα modulates microglial efferocytosis and neuroinflammation following experimental SAH via the SHP1/STAT6 axis. SAH induces extensive neuronal cell death, resulting in the release of DAMPs. These DAMPs, along with hemoglobin and cellular corpses, trigger localized inflammation. SIRPα inhibits efferocytosis by recruiting and phosphorylating SHP1 and SHP2 through the phosphorylation of four tyrosine residues in its cytoplasmic domain, with SHP1 playing a particularly critical role. Mutation of these tyrosine residues to alanine enhances efferocytosis and reduces neuroinflammation both in vivo and in vitro, through dephosphorylation of p-STAT6 and subsequent upregulation of the transcription of *Mertk* and *Cd36*

tyrosine phosphatases characterized by three structural domains: a protein tyrosine phosphatase (PTP) domain, two tandem SH2 domains (N-SH2 and C-SH2), and a C-terminal tail. In their unphosphorylated state, SHP1/2

are maintained in an auto-inhibited conformation, with the D'E loop of the N-SH2 domain extending into the catalytic cleft of the PTP domain [45, 46]. Upon binding of the SH2 domains to a specifically phosphorylated

tyrosine motif (such as that found in SIRP α), this inhibitory interaction is relieved, allowing the SHP1/2 substrates to enter the catalytic pocket, where dephosphorylation occurs, thereby mediating the subsequent inhibitory effect [47–49].

Similarly, under stimulation with 10 μ M Hb and ACs, we observed that the ITIMs of SIRP α became phosphorylated, leading to the recruitment and phosphorylation of SHP1 and SHP2, with a particular emphasis on SHP1. To further investigate this, we mutated the tyrosine residues at positions 440, 464, 481, and 505 in the intracellular region of SIRP α to alanine, a non-phosphorylatable amino acid. The SIRP α mutant exhibited enhanced phagocytic capacity and reduced recruitment of SHP1, as well as a diminished inflammatory response, compared to the wild-type. Additionally, in the SIRP α mutant microglia-neuron co-culture system, we observed a significantly higher number of surviving neurons and increased lysosomal acidity.

However, the precise mechanism by which SIRP α regulates efferocytosis and its downstream signaling through SHP1 remains to be elucidated. Therefore, we performed RNA sequencing comparing Ctrl and SIRP α mutant under stimulation with 10 μ M Hb and ACs. The results revealed differential gene expression, with significant enrichment in pathways related to inflammatory response. Notably, the “eat-me” signals *Mertk* and *Cd36* were significantly upregulated. Subsequently, we predicted and confirmed that STAT6 is the key transcription factor regulating *Mertk* and *Cd36* transcription, as demonstrated by ChIP and dual-luciferase reporter assays. Several members of the STAT family play crucial roles in regulating the functional status of microglia and macrophages [50]. Specifically, STAT6 signaling appears to promote the acquisition of an anti-inflammatory phenotype in microglia/macrophages [31, 51]. Additionally, IL-4, a STAT6 activator, drives microglia/macrophages toward a beneficial phenotype and supports stroke recovery [52]. Moreover, Co-IP assays confirmed STAT6 is a substrate of dephosphatase SHP1. Under SAH conditions, the ITIMs of SIRP α become phosphorylated, leading to the recruitment and phosphorylation of SHP1 and SHP2. Phosphorylated SHP1 dephosphorylates p-STAT6, preventing its translocation to the nucleus, thereby inhibiting its role as a key transcription factor for the “eat-me” signals *mertk* and *cd36*, ultimately suppressing efferocytosis.

There are several limitations in our study. First, our research focused exclusively on animal and cell models, specifically microglia, following SIRP α knockdown or mutation. Future experiments will include overexpression or similar interventions to further validate and strengthen our findings. Second, the specific stimulatory conditions under which SIRP α recruits either SHP1

or SHP2, as well as the regulatory consequences of differential SHP1 and SHP2 binding, have not been clearly elucidated. Finally, our study was conducted exclusively in male mice, which may limit the generalizability of our findings. Therefore, the influence of sex should be further investigated and considered in future studies.

In conclusion, our study demonstrates that SIRP α regulates efferocytosis and plays a significant role in neuroinflammation and EBI following SAH. After SAH, the ITIMs of SIRP α become phosphorylated, leading to the recruitment and phosphorylation of SHP1 and SHP2, with a particular emphasis on SHP1. Phosphorylated SHP1 dephosphorylates p-STAT6, preventing its translocation to the nucleus and thereby inhibiting its function as a key transcription factor for the “eat-me” signals *Mertk* and *Cd36*, which ultimately suppresses efferocytosis. Future research will focus on elucidating the precise mechanisms by which SIRP α recruits SHP1 or SHP2, as well as the regulatory consequences of differential SHP1 and SHP2 binding. These investigations will provide more detailed insights, which may contribute to the development of more targeted and effective therapeutic strategies.

Abbreviations

DAMPs	Damage-associated molecular patterns
SIRP α	Signal regulatory protein alpha
CSF	Cerebrospinal fluid
SAH	Subarachnoid hemorrhage
EBI	Early brain injury
DCI	Delayed cerebral ischemia
BBB	Blood-brain barrier
ACs	Apoptotic cells
ITIMs	Immunoreceptor tyrosine-based inhibitory motifs
SH2	Src homology region 2
DSA	Digital subtraction angiography
IL	1 β -Interleukin-1 β
IL	18-Interleukin-18
IL	10-Interleukin-10
TGF	β 1-Transforming growth factor- β
OxyHb	Oxyhemoglobin
CD47	Cluster of differentiation 47
SHP1	Src homology region 2 (SH2) domain-containing phosphatase 1
SHP2	Src homology region 2 (SH2) domain-containing phosphatase 2
STAT6	Signal transducer and activator of transcription 6
MerTK	Myeloid-epithelial-reproductive tyrosine kinase
CD36	Cluster of differentiation 36
IP	Immunoprecipitation
GAPDH	Glyceraldehyde-3-phosphate dehydrogenase
TUNEL	Terminal deoxynucleotidyl transferase
Neun	Neuronal nuclei
Iba1	Ionized calcium-binding adaptor molecule 1

Supplementary Information

The online version contains supplementary material available at <https://doi.org/10.1186/s12974-025-03414-6>.

Supplementary Material 1

Supplementary Material 2

Author contributions

B.Z. designed the experiments. B.Z., Y.Z., Z.Y. and Q.T. performed the experiments. B.Z., Z.Z. and K.J. analyzed raw data. S.C., Q.W., X.Z. and X.Z. reviewed the data and made substantial contributions to improving the studies. B. Z. and X.Z. wrote the manuscript. All the authors have contributed to the critical revision of the final manuscript.

Funding

This work was supported by grants from the National Natural Science Foundation of China (82071328).

Data availability

No datasets were generated or analysed during the current study.

Declarations

Competing interests

The authors declare no competing interests.

Received: 4 December 2024 / Accepted: 10 March 2025

Published online: 19 March 2025

References

- Hoh BL, Ko NU, Amin-Hanjani S, Chou S-Y, Cruz-Flores S, Dangayach NS, et al. 2023 guideline for the management of patients with aneurysmal subarachnoid hemorrhage: A guideline from the American heart association/american stroke association. *Stroke*. 2023;54(7):e314–70.
- Claassen J, Park S. Spontaneous subarachnoid haemorrhage. *Lancet*. 2022;400(10355):846–62.
- Etminan N, Chang HS, Hackenberg K, de Rooij NK, Vergouwen MDI, Rinkel GJE, et al. Worldwide incidence of aneurysmal subarachnoid hemorrhage according to region, time period, blood pressure, and smoking prevalence in the population: A systematic review and Meta-analysis. *JAMA Neurol*. 2019;76(5):588–97.
- Chen J, Li M, Liu Z, Wang Y, Xiong K. Molecular mechanisms of neuronal death in brain injury after subarachnoid hemorrhage. *Front Cell Neurosci*. 2022;16:1025708.
- Chen Y, Galea I, Macdonald RL, Wong GKC, Zhang JH. Rethinking the initial changes in subarachnoid haemorrhage: focusing on real-time metabolism during early brain injury. *EBioMedicine*. 2022;83:104223.
- Chen S, Feng H, Sherchan P, Klebe D, Zhao G, Sun X, et al. Controversies and evolving new mechanisms in subarachnoid hemorrhage. *Prog Neurobiol*. 2014;115:64–91.
- Lucke-Wold BP, Logsdon AF, Manoranjan B, Turner RC, McConnell E, Vates GE, et al. Aneurysmal subarachnoid hemorrhage and neuroinflammation: A comprehensive review. *Int J Mol Sci*. 2016;17(4):497.
- Serrone JC, Maekawa H, Tjahjedi M, Hernesniemi J. Aneurysmal subarachnoid hemorrhage: pathobiology, current treatment and future directions. *Expert Rev Neurother*. 2015;15(4):367–80.
- Doran AC, Yurdagul A Jr., Tabas I. Efferocytosis in health and disease. *Nat Rev Immunol*. 2020;20(4):254–67.
- Zhao Y, Luo Y, Liu Y, Lenahan C, Wu Q, Chen S. The role of autophagy and apoptosis in early brain injury after subarachnoid hemorrhage: an updated review. *Mol Biol Rep*. 2022;49(11):10775–82.
- Boada-Romero E, Martinez J, Heckmann BL, Green DR. The clearance of dead cells by efferocytosis. *Nat Rev Mol Cell Biol*. 2020;21(7):398–414.
- Ohashi SN, DeLong JH, Kozberg MG, Mazur-Hart DJ, van Veluw SJ, Alkayed NJ, et al. Role of inflammatory processes in hemorrhagic stroke. *Stroke*. 2023;54(2):605–19.
- Chaudhry SR, Hafez A, Rezaei Jahromi B, Kinfe TM, Lamprecht A, Niemela M et al. Role of damage associated molecular pattern molecules (DAMPs) in aneurysmal subarachnoid hemorrhage (aSAH). *Int J Mol Sci*. 2018;19(7).
- Jia J, Yang L, Chen Y, Zheng L, Chen Y, Xu Y, et al. The role of microglial phagocytosis in ischemic stroke. *Front Immunol*. 2021;12:790201.
- Liu J, Zhu Z, Leung GK. Erythrophagocytosis by microglia/macrophage in intracerebral hemorrhage: from mechanisms to translation. *Front Cell Neurosci*. 2022;16:818602.
- Bulters D, Gaastra B, Zolnourian A, Alexander S, Ren D, Blackburn SL, et al. Haemoglobin scavenging in intracranial bleeding: biology and clinical implications. *Nat Rev Neurol*. 2018;14(7):416–32.
- Schilperoort M, Ngai D, Sukka SR, Avramopoulos K, Shi H, Tabas I. The role of efferocytosis-fueled macrophage metabolism in the resolution of inflammation. *Immunol Rev*. 2023;319(1):65–80.
- Xu CR, Li JR, Jiang SW, Wan L, Zhang X, Xia L, et al. CD47 Blockade accelerates blood clearance and alleviates early brain injury after experimental subarachnoid hemorrhage. *Front Immunol*. 2022;13:823999.
- Logtenberg MEW, Scheeren FA, Schumacher TN. The CD47-SIRPalpha immune checkpoint. *Immunity*. 2020;52(5):742–52.
- Matozaki T, Murata Y, Okazawa H, Ohnishi H. Functions and molecular mechanisms of the CD47-SIRPalpha signalling pathway. *Trends Cell Biol*. 2009;19(2):72–80.
- Barclay AN, Van den Berg TK. The interaction between signal regulatory protein alpha (SIRPalpha) and CD47: structure, function, and therapeutic target. *Annu Rev Immunol*. 2014;32:25–50.
- Singla B, Lin HP, Ahn W, Xu J, Ma Q, Sghayer M, et al. Loss of myeloid cell-specific SIRPalpha, but not CD47, attenuates inflammation and suppresses atherosclerosis. *Cardiovasc Res*. 2022;118(15):3097–111.
- Shi H, Wang X, Li F, Gerlach BD, Yurdagul A, Moore MP, et al. CD47-SIRPalpha axis blockade in NASH promotes necroptotic hepatocyte clearance by liver macrophages and decreases hepatic fibrosis. *Sci Transl Med*. 2022;14(672):eabp8309.
- Tao C, Keep RF, Xi G, Hua Y. CD47 blocking antibody accelerates hematoma clearance after intracerebral hemorrhage in aged rats. *Transl Stroke Res*. 2020;11(3):541–51.
- Jing C, Bian L, Wang M, Keep RF, Xi G, Hua Y. Enhancement of hematoma clearance with CD47 blocking antibody in experimental intracerebral hemorrhage. *Stroke*. 2019;50(6):1539–47.
- Wang J, Ding X, Wu X, Liu J, Zhou R, Wei P, et al. SIRPalpha deficiency accelerates the pathologic process in models of Parkinson disease. *Glia*. 2019;67(12):2343–59.
- Zhang X, Wu Q, Zhang Q, Lu Y, Liu J, Li W, et al. Resveratrol attenuates early brain injury after experimental subarachnoid hemorrhage via inhibition of NLRP3 inflammasome activation. *Front Neurosci*. 2017;11:611.
- Yuan B, Zhou XM, You ZQ, Xu WD, Fan JM, Chen SJ, et al. Inhibition of AIM2 inflammasome activation alleviates GSDMD-induced pyroptosis in early brain injury after subarachnoid haemorrhage. *Cell Death Dis*. 2020;11(1):76.
- Zhang F, Zhou J, Lu P, Zhang X, Yang L, Wu J, et al. Lactylation of histone by BRD4 regulates astrocyte polarization after experimental subarachnoid hemorrhage. *J Neuroinflammation*. 2024;21(1):186.
- Zhang G, Li Q, Tao W, Qin P, Chen J, Wang H, et al. Sigma-1 receptor-regulated efferocytosis by infiltrating circulating macrophages/microglial cells protects against neuronal impairments and promotes functional recovery in cerebral ischemic stroke. *Theranostics*. 2023;13(2):543–59.
- Cai W, Dai X, Chen J, Zhao J, Xu M, Zhang L et al. STAT6/Arg1 promotes microglia/macrophage efferocytosis and inflammation resolution in stroke mice. *JCI Insight*. 2019;4(20).
- Chen X, Jiang M, Li H, Wang Y, Shen H, Li X, et al. CX3CL1/CX3CR1 axis attenuates early brain injury via promoting the delivery of Exosomal microRNA-124 from neuron to microglia after subarachnoid hemorrhage. *J Neuroinflammation*. 2020;17(1):209.
- Fang Y, Liu Y, Chen L, Wang J, Zhang J, Zhang H, et al. Cerebrospinal fluid markers of neuroinflammation and coagulation in severe cerebral edema and chronic hydrocephalus after subarachnoid hemorrhage: a prospective study. *J Neuroinflammation*. 2024;21(1):237.
- Bothwell SW, Janigro D, Patabendige A. Cerebrospinal fluid dynamics and intracranial pressure elevation in neurological diseases. *Fluids Barriers CNS*. 2019;16(1):9.
- Higginbotham L, Ping L, Dammer EB, Duong DM, Zhou M, Gearing M, et al. Integrated proteomics reveals brain-based cerebrospinal fluid biomarkers in asymptomatic and symptomatic Alzheimer's disease. *Sci Adv*. 2020;6(43):eaaz9360.
- Karayel O, Virreira Winter S, Padmanabhan S, Kuras YI, Vu DT, Tuncali I, et al. Proteome profiling of cerebrospinal fluid reveals biomarker candidates for Parkinson's disease. *Cell Rep Med*. 2022;3(6):100661.
- Zhang W, Zhao J, Wang R, Jiang M, Ye Q, Smith AD, et al. Macrophages reprogram after ischemic stroke and promote efferocytosis and inflammation resolution in the mouse brain. *CNS Neurosci Ther*. 2019;25(12):1329–42.

38. Chang CF, Goods BA, Askenase MH, Hammond MD, Renfro SC, Steinschneider AF, et al. Erythrocyte efferocytosis modulates macrophages towards recovery after intracerebral hemorrhage. *J Clin Invest*. 2018;128(2):607–24.
39. Kourtzelis I, Hajjishengallis G, Chavakis T. Phagocytosis of apoptotic cells in resolution of inflammation. *Front Immunol*. 2020;11:553.
40. Adkar SS, Leeper NJ. Efferocytosis in atherosclerosis. *Nat Rev Cardiol*. 2024;21(11):762–79.
41. Sakano Y, Sakano K, Hurrell BP, Shafiei-Jahani P, Kazemi MH, Li X, et al. SIRPalpha engagement regulates ILC2 effector function and alleviates airway hyperreactivity via modulating energy metabolism. *Cell Mol Immunol*. 2024;21(10):1158–74.
42. Grazda R, Seyfried AN, Maddipati KR, Fredman G, MacNamara KC. Resolvin E1 improves efferocytosis and rescues severe aplastic anemia in mice. *Cell Death Dis*. 2024;15(5):324.
43. Bouwstra R, van Meerten T, Bremer E. CD47-SIRPalpha blocking-based immunotherapy: current and prospective therapeutic strategies. *Clin Transl Med*. 2022;12(8):e943.
44. Takagane K, Umakoshi M, Itoh G, Kuriyama S, Goto A, Tanaka M. SKAP2 suppresses inflammation-mediated tumorigenesis by regulating SHP-1 and SHP-2. *Oncogene*. 2022;41(8):1087–99.
45. Anselmi M, Hub JS. Atomistic ensemble of active SHP2 phosphatase. *Commun Biol*. 2023;6(1):1289.
46. Buck SJS, Plaman BA, Bishop AC. Inhibition of SHP2 and SHP1 protein tyrosine phosphatase activity by chemically induced dimerization. *ACS Omega*. 2022;7(16):14180–8.
47. de Juan A, Tabtim-On D, Coillard A, Becher B, Goudot C, Segura E. The Aryl hydrocarbon receptor shapes monocyte transcriptional responses to interleukin-4 by prolonging STAT6 binding to promoters. *Sci Signal*. 2024;17(858):eadn6324.
48. Ming S, Li X, Xiao Q, Qu S, Wang Q, Fang Q et al. TREM2 aggravates sepsis by inhibiting fatty acid oxidation via the SHP1/BTK axis. *J Clin Invest*. 2024.
49. Fan D, Jiang WL, Jin ZL, Cao JL, Li Y, He T, et al. Leucine zipper protein 1 attenuates pressure overload-induced cardiac hypertrophy through inhibiting Stat3 signaling. *J Adv Res*. 2024;63:117–28.
50. Hu J, Liu W, Zou Y, Jiao C, Zhu J, Xu Q, et al. Allosterically activating SHP2 by oleanolic acid inhibits STAT3–Th17 axis for ameliorating colitis. *Acta Pharm Sinica B*. 2024;14(6):2598–612.
51. Szanto A, Balint BL, Nagy ZS, Barta E, Dezso B, Pap A, et al. STAT6 transcription factor is a facilitator of the nuclear receptor PPARγ-Regulated gene expression in macrophages and dendritic cells. *Immunity*. 2010;33(5):699–712.
52. Xu J, Chen Z, Yu F, Liu H, Ma C, Xie D, et al. IL-4/STAT6 signaling facilitates innate hematoma resolution and neurological recovery after hemorrhagic stroke in mice. *Proc Natl Acad Sci U S A*. 2020;117(51):32679–90.

Publisher's note

Springer Nature remains neutral with regard to jurisdictional claims in published maps and institutional affiliations.